

May 2026

IEA Wind TCP Task 49

**The IEA Wind RFA3
Deep-Water Reference
Array Design**



iea wind

**Prepared for the
IEA Wind TCP**



May 2026

Authors:

Ericka Lozon

IEA Wind Task 49, United States

Vishnu R. N. Rajasree

Norwegian University of Science and Technology, Norway

Daniel Mulas Hernando

IEA Wind Task 49, United States

Junho Lee

Deep Anchor Solutions Inc., United States

Michel Castagné

IFP Energies nouvelles, France

Alice Nassor

IFP Energies nouvelles, France

Yann Poirette

IFP Energies nouvelles, France

Yuksel Rudy Alkarem

IEA Wind Task 49, United States

Leah Sirkis

IEA Wind Task 49, United States

Matthew Hall

SINTEF, Norway

IEA Wind TCP functions within a framework created by the International Energy Agency (IEA). Views, findings, and publications of IEA Wind do not necessarily represent the views or policies of the IEA Secretariat or of all its individual member countries. IEA Wind is part of IEA's Technology Collaboration Programme (TCP).

Acknowledgments

This report is a product of International Energy Agency Wind Technology Collaboration Programme (IEA Wind) Task 49 on Integrated Design of Floating Wind Arrays. This research benefited from the collaboration of many individuals and institutions, including Malcolm Bowie, Madhan Mohan, Vimal Vinayan, Erin Bachynski-Polić, and Thomas Sauder. The engagement of all participants in Task 49 Work Package 2 and additional review from other participants in Task 49 is gratefully acknowledged.

The contribution from the Norwegian University of Science and Technology (NTNU) is funded by the Research Council of Norway through the project 326654 CYBERLAB KPN, a collaboration between SINTEF Ocean, NTNU, University of Aarhus, Equinor, Mainstream Renewable Power, APL Norway, Sevan Deepwater Technology, and Delmar Systems.

The contribution from IFP Energies nouvelles (IFPEN) is funded by Agence pour le Développement et la Maitrise de l’Energie (ADEME), the French Environment and Energy Management Agency.

List of Acronyms

ABS	American Bureau of Shipping
AEP	annual energy production
AHT	anchor handling tug
API	American Petroleum Institute
BOS	balance of system
CapEx	capital expenditures
CLV	cable lay vessel
CTV	crew transfer vessel
DLC	design load case
DSV	diving support vessel
FCR	fixed charge rate
FLORIS	FLOW Redirection and Induction in Steady State
GW	gigawatt
IEA	International Energy Agency
IEC	International Electrotechnical Commission
IFPEN	IFP Energies nouvelles
kg	kilogram
km	kilometer
kN	kilonewton
LCOE	levelized cost of energy
m	meter
MBL	minimum bearing load
MBR	minimum bending radius
mm	millimeter
MW	megawatt
MWh	megawatt-hour
N	newton
NLR	National Laboratory of the Rockies
O&M	operations and maintenance
OCS	Outer Continental Shelf
OpEx	operational expenditures
ORBIT	Offshore Renewables Balance-of-System and Installation Tool
OSS	offshore substation
POI	point of interconnection
SLC	survival load case
TLP	tension-leg platform
USD	U.S. dollar
WACC	weighted average cost of capital
WAVES	Wind Asset Value Estimation System
WOMBAT	Windfarm Operations and Maintenance cost-Benefit Analysis Tool

Executive Summary

This report presents a deep-water floating wind array reference design developed under Task 49 of the International Energy Agency Wind Technology Collaboration Programme (IEA Wind). This design is the task's first reference floating array (RFA) produced for deep water and is given the name IEA Wind RFA3. Following the initial Task 49 scoping, the deep-water design is a 1-GW floating wind farm composed of 67 IEA Wind 15-MW reference turbines on University of Maine VoltturnUS-S reference semisubmersible platforms. The array is designed for a uniform 800-m water depth in meteorological and oceanographic conditions representative of Humboldt Bay, California. The design includes taut mooring systems with suction pile anchors and both fully suspended and lazy-wave dynamic power cable profiles. The array layout is rectangular and uniform, fitting within an area of 256 km².

The developed mooring design is composed primarily of polyester rope, with short sections of chain at the anchor and platform connections. The mooring design was primarily challenged by a constraint preventing slack loads on the mooring lines. To avoid the mooring lines losing tension, a clump weight was integrated along each polyester mooring line section. The mooring design performance was verified in dynamic simulations of both extreme and fatigue load cases to ensure that design constraints were met, and the lines were adequately sized. Additionally, suction caisson anchors were sized to withstand the mooring loads in extreme conditions. The dimensions of the anchor were selected to balance considerations in holding capacity, material efficiency, and installability.

Fully suspended and lazy-wave dynamic cable configurations were designed for three conductor sizes: 300, 630, and 1,000 mm². The dynamic cable designs were particularly challenged by the need to withstand the weight of marine growth and drag loads from extreme currents. The performance of the cable designs was verified in extreme load cases to check extreme tension and curvature constraints.

The array layout is a uniform grid. The grid spacing and orientation were iteratively varied and selected to maximize spacing in the north-south direction, which is the direction of the predominant wind resource in the Humboldt region. The mooring systems are oriented such that they are 180° opposing orientations in alternating columns, allowing the mooring systems to slot together and avoid crossing over each other. The cable routing was selected to route along turbine rows with fully suspended cables connecting adjacent turbines. Lazy-wave cables are used in some places to avoid mooring lines or facilitate connection to the substation, which is on the east side of the array.

The cost and logistics assessment follows a transparent, open-source methodology and set of assumptions used to evaluate the deep-water design, accounting especially for the effects of the mooring, cable, and layout design choices. The analysis applies process-based models for installation and operations and maintenance logistics as well as a wake and annual energy production model. These tools are used to estimate costs and generation and the resulting levelized cost of energy (LCOE). The LCOE for the 1-GW floating wind farm is estimated to be \$122.4/MWh (real 2024 U.S. dollars).

This deep-water floating wind array reference design is the product of a collaborative design effort across Norway, France, and the United States. To ease the use of this design, input files and design details are shared on GitHub, including in the Task 49 Ontology format. In this report, the design methodology and details are shared to provide a baseline and starting point to facilitate future research and development efforts on floating wind technology at the array scale in deep water.

Table of Contents

Executive Summary	v
1 Introduction	1
2 Site Conditions	3
3 Mooring Design	6
3.1 Design Assumptions and Requirements	6
3.2 Design Approach	7
3.3 Mooring Design Description	8
3.4 Performance Results	12
3.4.1 Maximum Tension	12
3.4.2 Line Slackness	13
3.4.3 Rope Zero Ground Contact	13
3.4.4 Maximum Horizontal Platform Displacement	14
3.4.5 Fatigue Criteria	14
4 Anchor Design	17
4.1 Design Assumptions and Requirements	17
4.2 Design Approach	17
4.3 Anchor Design Description	18
4.4 Performance Results	19
5 Dynamic Cable Design	21
5.1 Design Assumptions and Requirements	21
5.2 Design Approach	22
5.3 Suspended Cable Design Descriptions	23
5.4 Lazy-Wave Cable Design Descriptions	24
5.5 Performance Results	26
5.5.1 Maximum Tensions	26
5.5.2 Maximum Curvature	27
6 Layout	30
7 Cost and Logistics Modeling	36
7.1 Methodology	36
7.2 Assumptions	37
7.2.1 Plant Characteristics Summary	38
7.2.2 Task 49 Design Basis Cost and Logistics Considerations	39
7.3 Results 41	
7.3.1 FCR	41
7.3.2 CapEx	42
7.3.3 OpEx	43
7.3.4 Net AEP	44
7.3.5 LCOE	45
8 Conclusion	46
References	47

List of Figures

Figure 1. Humboldt lease area depths.....	3
Figure 2. Humboldt site (a) wind rose, (b) wave rose, and (c) current rose.....	4
Figure 3. Environment headings used for strength load cases.....	8
Figure 4. VoltturnUS-S platform and deep-water mooring system.....	8
Figure 5. Diagram of mooring line type sections (s1–s6) that correspond to the properties listed in Table 7.....	10
Figure 6. Line tension statistics.....	12
Figure 7. Tension safety factor for mooring line 2 for 0° environmental heading.....	13
Figure 8. Statistics of the vertical height of the top of the bottom chain from the seafloor.....	14
Figure 9. Statistics of the platform horizontal displacement.....	14
Figure 10. Accumulated fatigue damage for different platform orientations.....	15
Figure 11. Driving environmental loading directions used in dynamic cable simulations.....	23
Figure 12. Suspended cable profiles for conductor sizes of (a) 300-mm ² , (b) 630-mm ² , and (c) 1,000-mm ² conductor sizes.....	23
Figure 13. Lazy-wave cable profile at 0 m, -45 m, and 45 m offsets.....	25
Figure 14. Suspended cable tensions for (a) 300-mm ² , (b) 630-mm ² , and (c) 1,000-mm ² conductor sizes.....	26
Figure 15. Lazy-wave cable tensions for (a) 300-mm ² , (b) 630-mm ² , and (c) 1,000-mm ² conductor sizes.....	27
Figure 16. Suspended cable maximum curvature for (a) 300-mm ² , (b) 630-mm ² , and (c) 1,000-mm ² conductor sizes.....	28
Figure 17. Violin plots of suspended cable curvature in SLC 90° for (a) 300-mm ² , (b) 630-mm ² , and (c) 1,000-mm ² conductor sizes.....	28
Figure 18. Lazy-wave maximum curvature for (a) 300-mm ² , (b) 630-mm ² , and (c) 1,000-mm ² conductor sizes.....	29
Figure 19. Violin plots of lazy-wave cable curvature in SLC 180° for (a) 300-mm ² , (b) 630-mm ² , and (c) 1,000-mm ² conductor sizes.....	29
Figure 20. Spatial constraints around mooring lines and platforms for layout optimization [24].....	30
Figure 21. Parameterization of regular, gridded array layout [1].....	31
Figure 22. Array layout and cable routing.....	33
Figure 23. Three-dimensional view of the deep-water array design.....	33
Figure 24. Reference site located within the Humboldt lease areas (OCS-P 0561 and OCS-P 0562), showing assumed routes and calculated distances used for cost and logistics modeling.....	39
Figure 25. CapEx donut chart, showing each component’s share of total CapEx.....	43
Figure 26. LCOE waterfall in real 2024 USD.....	45
Figure A-1. Gumbel distribution fit for maximum tension in mooring line 2, DLC 1.6, 0°.....	51
Figure A-2. Gumbel distribution fit for maximum tension in mooring line 2, DLC 6.1, 0°.....	51
Figure A-3. Gumbel distribution fit for maximum tension in mooring line 2, SLC, 0°.....	51

List of Tables

Table 1. Proposed Deep-Water Design Scenarios and Features [1].....	1
Table 2. Metocean Parameters for Critical Strength Load Cases.....	4
Table 3. Current Profiles at Different Return Periods.....	5
Table 4. Assumed Thickness of Marine Growth at Depth Ranges.....	5
Table 5. Mooring Design Criteria.....	6
Table 6. Mooring Design Parameters.....	9
Table 7. Mooring Line Properties Including Marine Growth.....	11
Table 8. Final Suction Anchor Configuration and Verification Summary.....	19

Table 9. Dynamic Cable Properties	21
Table 10. Buoyancy Module Properties.....	21
Table 11. Suspended Cable Design Parameters.....	24
Table 12. Suspended Cable Parameters With Marine Growth	24
Table 13. Lazy-Wave Cable Design Parameters.....	25
Table 14. Lazy-Wave Cable Parameters With Marine Growth	26
Table 15. Array Layout and Mooring Line Orientation Parameters.....	32
Table 16. Turbine and Substation Coordinates.....	34
Table 17. Summary of Design Basis Considerations by Key LCOE Driver	40
Table 18. Cost and Mass of Taut Line (Chain-Clump Weight-Polyester-Chain) With 1,400-m Anchoring Radius	40
Table 19. Cost and Mass of Suction Pile Anchor	40
Table 20. Cost and Mass of 66-kV Array Cables	41
Table 21. Inputs and Outputs Used To Derive FCR.....	41
Table 22. CapEx Breakdown in 2024 USD	42
Table 23. OpEx Breakdown in 2024 USD.....	44
Table 24. Breakdown of Losses From Gross to Net Generation	45

1 Introduction

International Energy Agency Wind Technology Collaboration Program (IEA Wind) Task 49 focuses on the Integrated Design of Floating Wind Arrays. Within Task 49, Work Package 2 aims to produce reference array designs for characteristic sites that will further floating wind research efforts at the array scale. Through a collaborative brainstorming effort, the Work Package 2 team outlined three initial reference floating array (RFA) design scenarios for shallow, intermediate, and deep-water depths. Each design scenario focuses on addressing various critical challenges for floating wind, and the resulting designs are labeled IEA Wind RFA1, RFA2, and RFA3. The scope of each design consists of using existing turbine and platform reference designs, developing new mooring system and dynamic cable designs, setting the array layout, and sizing and routing all intra-array power cables to an assumed substation position (the substation itself is not included in the design).

The proposed deep-water design scenario was planned to feature deep-water innovations, such as taut fiber-rope mooring lines and fully suspended power cables, at a uniform 800-m water depth. The features of the planned deep-water design are shown in Table 1. The table also lists potential future variants, such as depth gradients, shared moorings, and tension-leg platforms (TLPs).

Table 1. Proposed Deep-Water Design Scenarios and Features [1]

Scenario	Description
Key features	Deep-water constraints on mooring layout and turbine spacing, use of W-shaped cables and deep-water mooring innovations
Design variants (sequential)	V1: uniform Secondary options: V2: depth gradient with adapted layout, moorings, cables V3: shared mooring option V4: TLP option
Metocean	Humboldt
Depth	800 m Secondary option: irregular 600–1,000 m
Seabed	Generic
Array layout	Rectangular Secondary option: varied
Platform type	Semi or spar Secondary option: TLP
Mooring configuration	Taut synthetic Secondary options: shared taut, TLP
Mooring layout	Regular
Anchors	Suction pile Secondary option: drag embedment
Cable configuration	Fully suspended

Through a collaborative effort across an international design team, we developed the first variant of the Task 49 deep-water design. The IEA Wind RFA3 design is a 1-GW floating wind farm, consisting of 67 IEA Wind 15-MW turbines [2] with reference VoltturnUS-S semisubmersible platforms [3]. Following the design scoping in Table 1, the design features a rectangular array layout in 800-m water depth with site conditions based on the Humboldt wind energy area in California. The mooring systems are taut with suction anchors. For the dynamic power cables, fully suspended configurations are used where possible considering the significant water depth. The deep-water design was developed following the requirements and methodology outlined in *The IEA Wind Task 49 Reference Floating Wind Array Design Basis* [1].

This report describes the methodology and details of the Task 49 deep-water design. Section 2 outlines the site conditions. Section 3 describes the taut fiber-rope mooring system. Section 4 presents the suction anchor design. Section 5 describes the intra-array dynamic cables, including both fully suspended and lazy-wave designs. Section 6 details the wind farm layout, turbine positions, and cable routing. Finally, Section 7 shares cost modeling assumptions, methodology, and results.

2 Site Conditions

The Task 49 deep-water design adopted site conditions that are representative of the Humboldt wind energy area off the coast of California. The Humboldt lease areas have water depths ranging from 550 to 1,300 m, as shown in Figure 1. For the array design, a uniform depth of 800 m was assumed. In previous work, meteorological and oceanographic (metocean) data for Humboldt were gathered from various sources, including metocean buoys operated by the National Data Buoy Center and the 2023 National Offshore Wind Data Set. The data were processed into extreme wind, wave, and current parameters at various return periods as well as fatigue bins, contributing to a set of reference site conditions based on the Humboldt location [4],[5]. These conditions are also included in the global reference site condition sets developed in Task 49 [6].

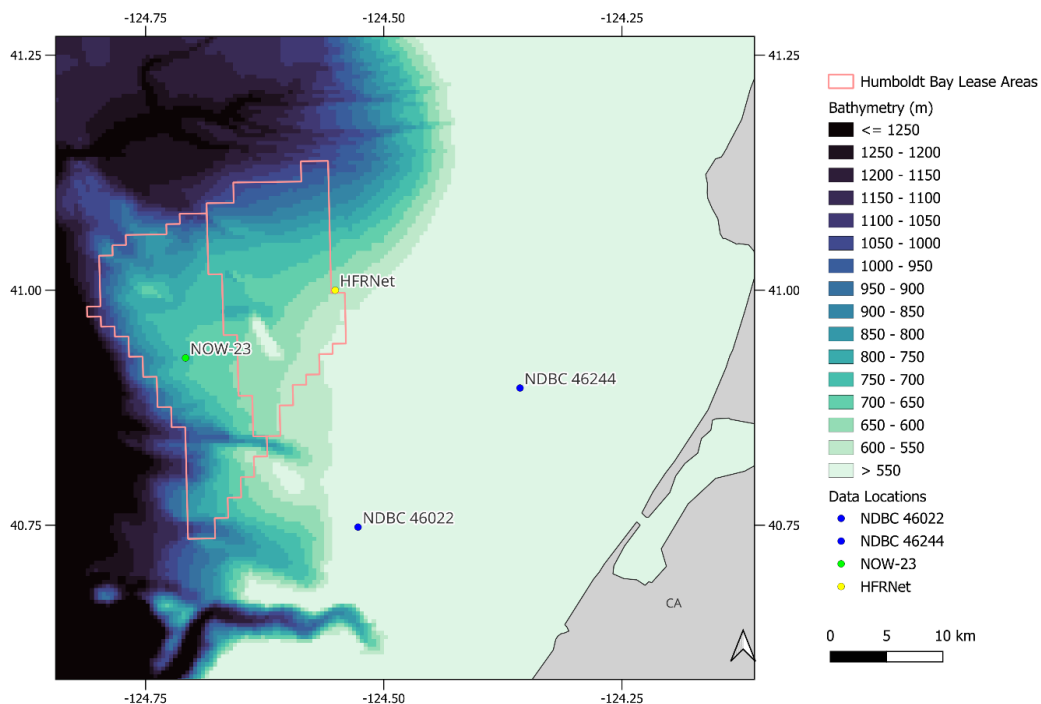


Figure 1. Humboldt lease area depths.

NDBC = National Data Buoy Center; NOW-23 = 2023 National Offshore Wind Data Set; HFRNet = High-Frequency Radar Network

The Humboldt wind, wave, and current roses are shown in Figure 2.

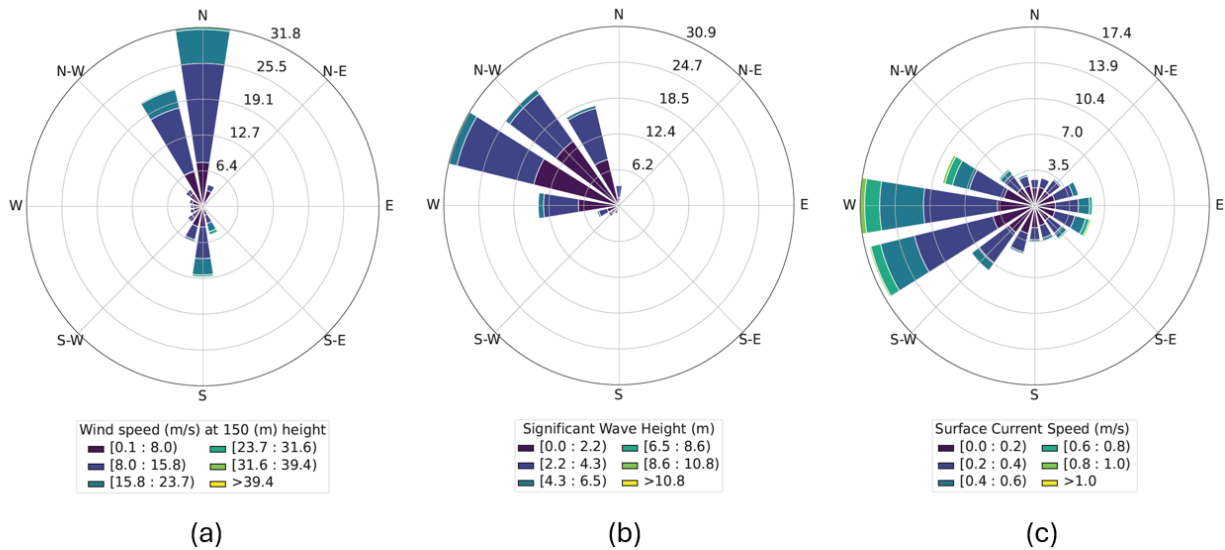


Figure 2. Humboldt site (a) wind rose, (b) wave rose, and (c) current rose

The processed metocean data were extracted for critical load cases that were used to evaluate the performance of the mooring, anchor, and cable designs. The critical load cases were determined in [1] and include International Electrotechnical Commission (IEC) design load cases (DLCs) 1.6 and 6.1 and the survival load case (SLC) to assess the strength of the design in extreme metocean conditions. DLC 1.6 with rated wind speed exhibits maximum aerodynamic turbine thrust force along with severe waves. DLC 6.1 is a 50-year storm condition with a parked turbine. The SLC is a 500-year storm condition with lower safety factors. The metocean conditions for the critical load cases are shown in Table 2. Additionally, for the mooring design, DLC 1.2 was considered. DLC 1.2 consists of a range of metocean conditions and is used to assess lifetime damage.

Table 2. Metocean Parameters for Critical Strength Load Cases

Parameter	DLC 1.6	DLC 6.1	SLC
Wind speed (m/s)	10.59	39.44	42.97
Turbulence intensity	0.06	0.05	0.05
Shear	0.14	0.11	0.11
Wave height (m)	10.5	11.8	13.7
Wave period (s)	18.7	19.8	21.3
Current speed (m/s)	0.83	1.24	1.43
Safety factor	2	2	1.05

During the design process, the design team determined that additional current profile information was needed. The current profile with depth was shown to have a large impact on the dynamic cable tensions and performance. Additional current information was obtained from the Hybrid Coordinate Ocean Model (HYCOM) at several depths. Independent extremes were extrapolated

at each depth to develop conservative current profiles at various return periods. These current profiles are shown in Table 3.

Table 3. Current Profiles at Different Return Periods

Depth	1-year	50-year	500-year
Surface	0.83	1.24	1.43
10 m	0.64	1.01	1.21
50 m	0.47	0.86	1.12
100 m	0.39	0.67	0.85
800 m	0.11	0.15	0.16

Additionally, the marine growth assumptions from the design basis were adjusted slightly during the design process. The marine growth assumptions in design standards are not expected to be adequate for the deep water of the Humboldt region. Thus, the assumptions were adjusted so that zero marine growth was assumed below a depth of 170 m, based on the data in Devantier, Wong, and Schrameyer [7]. This adjustment was needed to allow for the development of suspended power cable designs within allowable tension limits. The final assumed marine growth thickness and depth ranges are shown in Table 4. The density of the marine growth is 1,325 kg/m³.

Table 4. Assumed Thickness of Marine Growth at Depth Ranges

Depth Range	Marine Growth Thickness (mm)
Surface–40 m	100
40–170 m	50
Below 170 m	0

3 Mooring Design

The taut fiber-rope mooring design was selected based on its suitability to the 800-m water depths of the site. Taut mooring systems are composed primarily of synthetic fiber rope, which provides restoring force through the elasticity of the material. Polyester has commonly been used in taut deep-water mooring designs, in various floating offshore energy applications.

3.1 Design Assumptions and Requirements

The mooring design requirements were identified in the design basis [1]. In the deep-water design, American Bureau of Shipping (ABS) guidelines [8] are primarily followed. In addition to the design requirements from the design basis [1], a slack constraint was also included in the design process, which ensures that the mooring lines do not reach zero tension. This constraint was based on extensive discussions within the Task 49 Work Package 2 team, which concluded that zero-tension events should be avoided because of possible snap loading events [9].

The criteria used for the mooring design are summarized in Table 5.

Table 5. Mooring Design Criteria

Criteria	Requirement
Maximum tension	<p>The design tension safety factor (SF) requirement per ABS guidelines [8] for nonredundant stationkeeping systems must follow these guidelines:</p> <ul style="list-style-type: none"> • SF > 2 for DLC 1.6 and DLC 6.1 • SF > 1.05 for SLC <p>where SF is defined as the ratio of minimum breaking load (MBL) of the mooring line to maximum tension value (MPV):</p> $SF = \frac{MBL}{MPV}$ <p>The design tension is defined as the most probable MPV obtained from extreme value distribution of peak tensions. The extreme tension distribution is constructed by fitting Gumbel distribution to the maximum tension obtained from 30 1-hour realizations.</p>
Line slackness	The minimum tension in the line must be greater than a nominal value of 100 kN for DLC 1.6 and DLC 6.1.
Rope zero ground contact	The polyester segments may not contact the seafloor (to avoid abrasion).
Maximum horizontal platform displacement	The maximum horizontal displacement of the platform must be less than 10% of the water depth (80 m).
Fatigue	The fatigue safety factor must be greater than 3, considering a 25-year lifetime.

3.2 Design Approach

A simple taut mooring design composed of alternating chain, polyester, and chain line sections was initially investigated. We tested various combinations of line diameters, chain and polyester section lengths, and anchor spacing; however, all these cases resulted in slack in the mooring lines near the anchor in DLCs 1.6 and 6.1. The slack events could be mitigated by setting the pretension to values greater than 3,000 kN, which led to larger line diameters and raised concerns about installation challenges. This motivated an investigation into using clump weights or buoys along the mooring line to mitigate the occurrence of slack events while maintaining reasonable pretension levels.

We iteratively evaluated different sizes and locations of clump weights and buoys along the line. The use of a buoy at the top of the bottom chain also successfully mitigated the slack with reasonable pretension of approximately 1,800 kN; however, based on feedback from the Task 49 team, the underwater buoy was considered expensive and difficult to install, maintain, and repair. Therefore, a design with a clump weight was developed instead. The sizing and location of the clump weight were based on a parametric study using static calculations in the quasi-static mooring model MoorPy [10], and the dynamic performance was then verified using OpenFAST.

The dynamic simulations were performed using:

- OpenFAST v4.0.4¹
- IEA 15-MW reference wind turbine model (v1.1.17 corresponding to commit 7106d3d, dated 21 March 2025)²
- ROSCO controller v2.9.0.³

The following assumptions/simplifications were made in the dynamic simulations in OpenFAST:

- For strength load cases, wind, wave, and current loads were considered, whereas for fatigue load cases, current was ignored. This simplification, aimed at reducing the number of metocean variables to be considered while the fatigue bins were produced, is based on the sensitivity study in [4], which indicated that the variation in fatigue damage for a taut mooring system in the cases with and without current was found to be within 1%. The current loading on the platform for strength load cases is applied as a constant load, calculated as $F_{current} = b \times v_c^2$ where b is the surge/sway quadratic damping coefficient ($b = 9.23E+05 \frac{N \cdot s^2}{m^2}$) and v_c is the surface current velocity.
- For the strength load cases, wind, wave, and current were assumed to be aligned. Two environmental headings were considered: 0° (loading with a mooring line directly upwind) and 180° (loading with a mooring line directly downwind), as shown in Figure 3. For fatigue load cases, the wind and wave directions are determined by the fatigue bins [4].

¹ <https://github.com/OpenFAST/openfast/releases/tag/v4.0.4>

² <https://github.com/IEAWindSystems/IEA-15-240-RWT/commit/7106d3d1cb990e43b4f6898554e1d4722a59dbc1>

³ <https://github.com/NREL/ROSCO/releases/tag/v2.9.0>

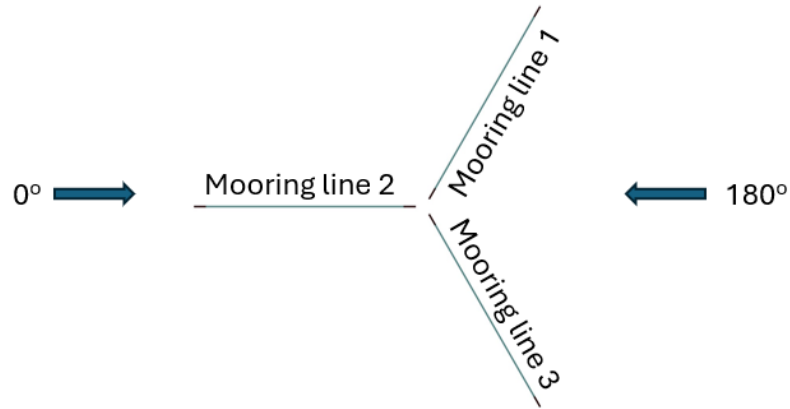


Figure 3. Environment headings used for strength load cases

- The hydrodynamic loads on mooring lines ignore the wave kinematics.
- Quadratic transfer functions for the OpenFAST model are only available for the 0° environmental heading. Hence, the second-order wave loads are only considered in the strength load cases with an environmental heading of 0°.

3.3 Mooring Design Description

A taut mooring system featuring a clump weight was designed for the site, as shown in Figure 4. It consists of three chain-polyester-chain segments spread 120 degrees apart. The clump weight is located on the polyester line section, roughly one-third the distance from the anchor chain attachment. The mooring design is described in

Table 6.

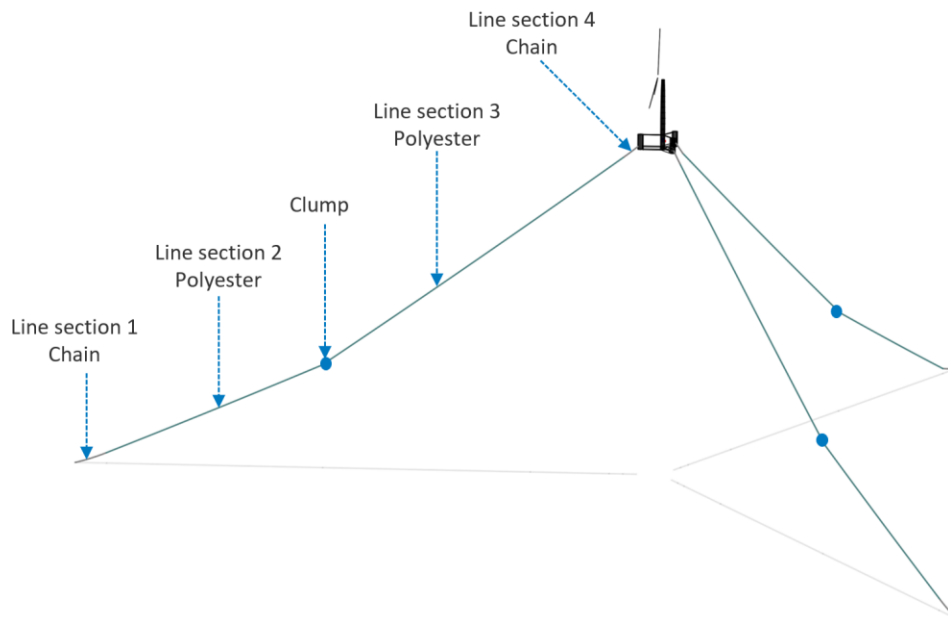


Figure 4. VoltturnUS-S platform and deep-water mooring system

The mooring line properties were calculated using the regression equations presented in the design basis [1]. Considering the varying thickness of marine growth with water depth and the position of the clump weight, each mooring line is divided into six sections, as shown in Figure 5. The marine growth, corrosion, and line properties for each segment are presented in Table 7.

Table 6. Mooring Design Parameters

Design Parameter	Value
Number of lines	3
Water depth	800 m
Anchor radius	1400 m
Fairlead radius	58 m
Fairlead depth	14 m
Initial pretension	2,070 kN
Line section 1 type	142 mm studless R4 chain
Line section 1 length	80 m
Line section 2 type	200 mm polyester
Line section 2 length	560 m
Clump weight mass	40 ton
Line section 3 type	200 mm polyester
Line section 3 length	870 m
Line section 4 type	142 mm studless R4 chain
Line section 4 length	40 m
Surge/sway natural period	149 s
Yaw natural period	84 s

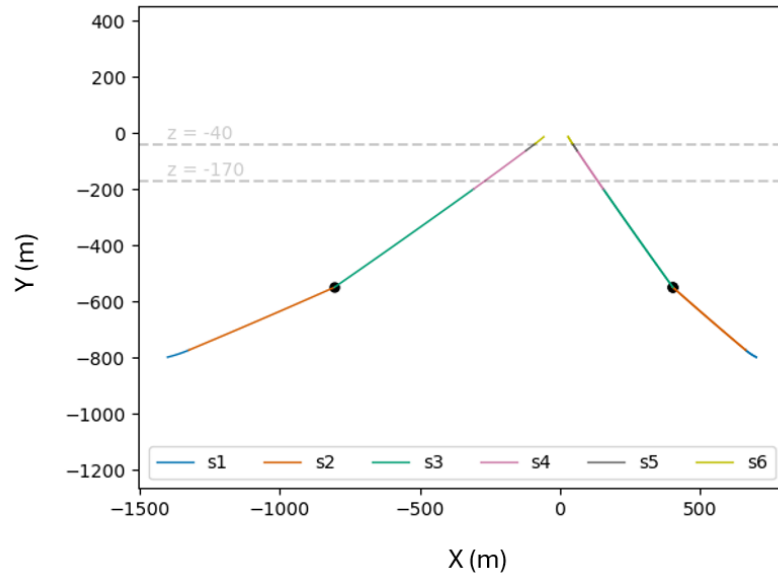


Figure 5. Diagram of mooring line type sections (s1–s6) that correspond to the properties listed in Table 7

Table 7. Mooring Line Properties Including Marine Growth

Section	Type	MBL^a (kN)	Nominal Diameter (mm)	Marine Growth (mm)	Corrosion Allowance (mm)	Unstretched Length (m)	Volumetric Diameter (m)	Mass Density (kg/m)	Static Elastic Stiffness (N)
S1	Chain	18,127	142	0	10	80	0.2556	403.28	1.726e+09
S2	Polyester	12,320	200	0	-	560	0.1580	27.16	1.725E+08
S3	Polyester	12,320	200	0	-	601	0.1580	27.16	1.725E+08
S4	Polyester	12,320	200	50	-	229	0.2738	79.19	1.725E+08
S5	Polyester	12,320	200	100	-	40	0.3807	152.04	1.725E+08
S6	Chain	18,127	142	100	10	40	0.5089	604.75	1.726e+09

^a The MBL value for chain presented in the table is the value without correction for corrosion allowance

For the polyester lines, the stiffness is modeled using a visco-elastic approach [11], in which the stiffness varies between static stiffness and dynamic stiffness based on the strain rate. The static stiffness is specified in Table 7, whereas the dynamic stiffness for each segment is set based on the mean tension of the segment in the particular loading condition. The design basis [1] provides a linear relationship between the mean tension and the dynamic stiffness.

3.4 Performance Results

Thirty 1-hour realizations of each strength load case (DLC 1.6, DLC 6.1, and SLC) were simulated in OpenFAST. For fatigue load cases, only one 1-hour realization was simulated. All the simulations were 4,200 s in length, with the first 600 s removed from statistical calculations to allow for transient dissipation. The results are summarized in the next sections.

3.4.1 Maximum Tension

The statistics of the mooring line tension over the realizations are presented in Figure 6. In the plot, the mean and standard deviation are calculated as the averages of the mean and standard deviation over the realizations. The minimum and maximum values, however, represent the extreme values observed across all realizations. The largest tension response is observed in mooring line 2 in the 0° environmental heading for each load case, which is the limiting case for design tension determination. The 0° environmental heading positions mooring line 2 directly upwind, resulting in maximum loads.

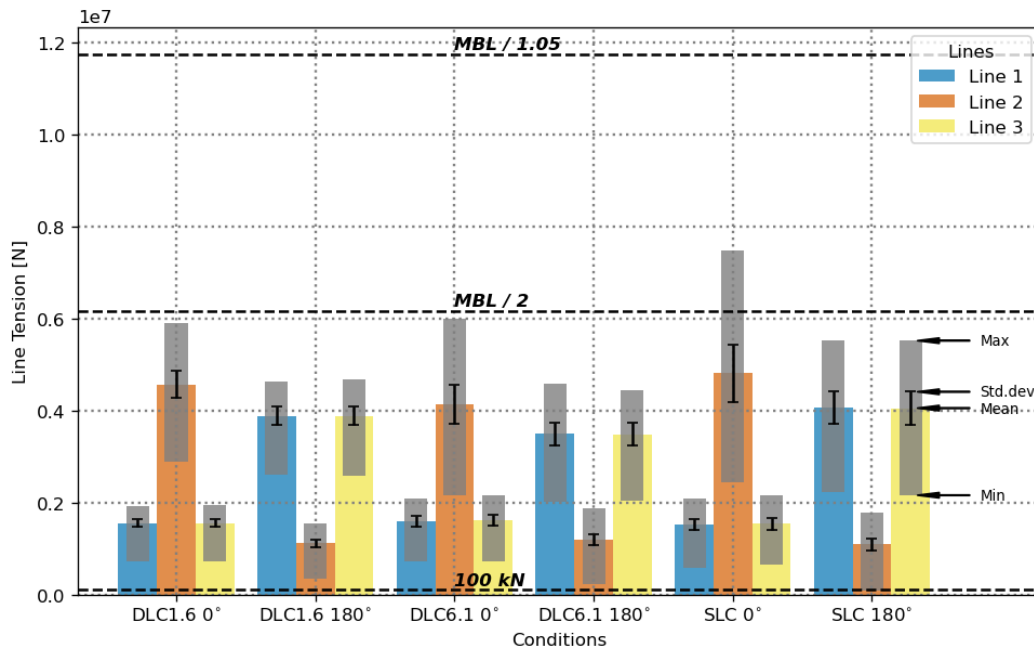


Figure 6. Line tension statistics

The Gumbel extreme value distribution is fit to the maximum tension values obtained from each realization to obtain the most probable maximum tension, which corresponds to the location parameter of the Gumbel distribution. The convergence of the location parameter against the number of seeds, as well as the fit probability density functions for the worst-case, zero-degree environmental headings for mooring line 2, are presented in . Based on the calculated most

probable maximum tension, the safety factor is calculated. The MBL of the polyester line is used in the calculation of the safety factor, as it is lower than that of the chain after considering 10 mm of corrosion allowance. The safety factors are presented in Figure 7 along with the ABS requirements. In both DLC 1.6 and DLC 6.1, the safety factors are greater than 2, and for SLC the safety factor is 1.783 (>1.05).

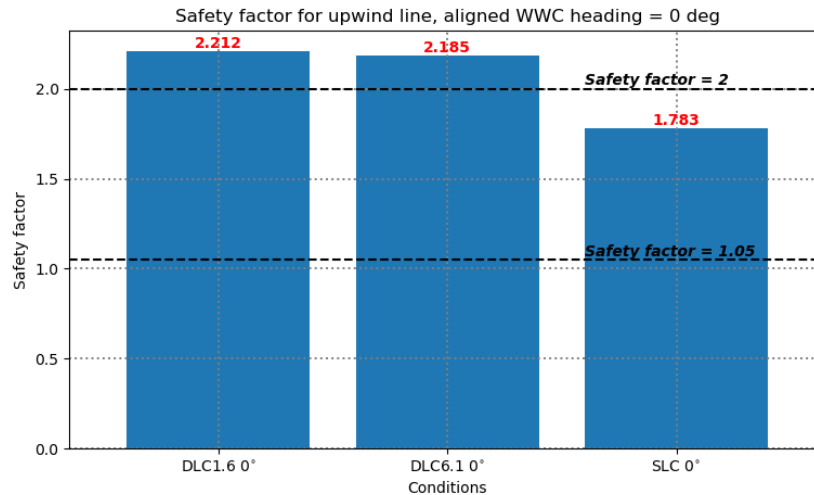


Figure 7. Tension safety factor for mooring line 2 for 0° environmental heading

3.4.2 Line Slackness

The minimum line tensions observed over all realizations are also shown in Figure 6. An environmental heading of 180° for mooring line 2 represents the limiting case for line slackness for every load case, as this heading positions a mooring line directly downwind of the environmental loading. For both DLC 1.6 and DLC 6.1, the minimum tension observed remains above a nominal value of 100 kN, as required. The tension falls below this limit in the SLC; however, this is considered to be acceptable due to the very low 500-year return period.

3.4.3 Rope Zero Ground Contact

The statistics of the vertical height of the node at the top of the bottom chain over all realizations are presented in Figure 8. For each load case, the environmental heading of 180° for mooring line 2 is the limiting case because it positions a mooring line directly downwind of the environmental loading. For both DLC 1.6 and DLC 6.1, the minimum height remains above 3.7 m, and for the SLC it remains above 1.54 m; hence, no polyester contact with the seafloor occurs in the simulations.

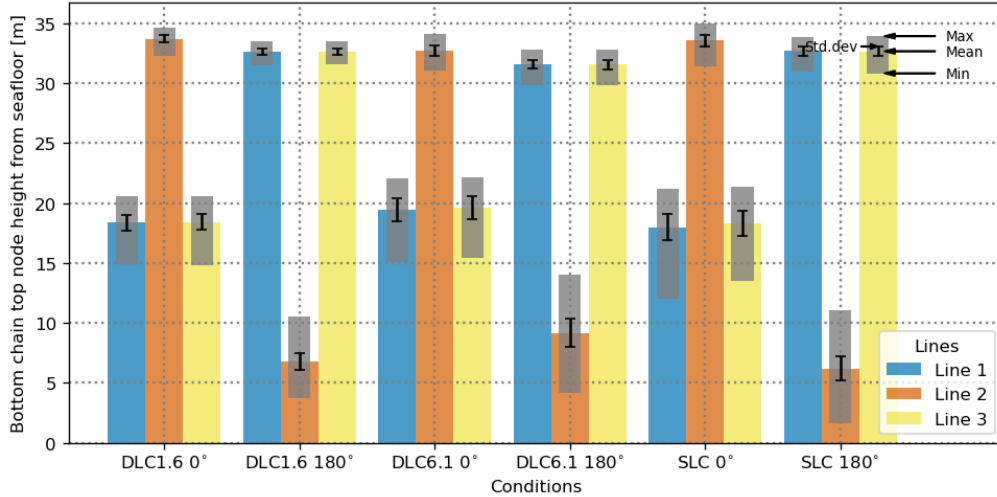


Figure 8. Statistics of the vertical height of the top of the bottom chain from the seafloor

3.4.4 Maximum Horizontal Platform Displacement

The statistics of maximum horizontal platform displacement across all realizations are presented in Figure 9. For each load case, the environmental heading of 180° represents the limiting case with the worst-case maximum displacement of approximately 69 m in the SLC, which is less than 10% of the water depth (80 m).

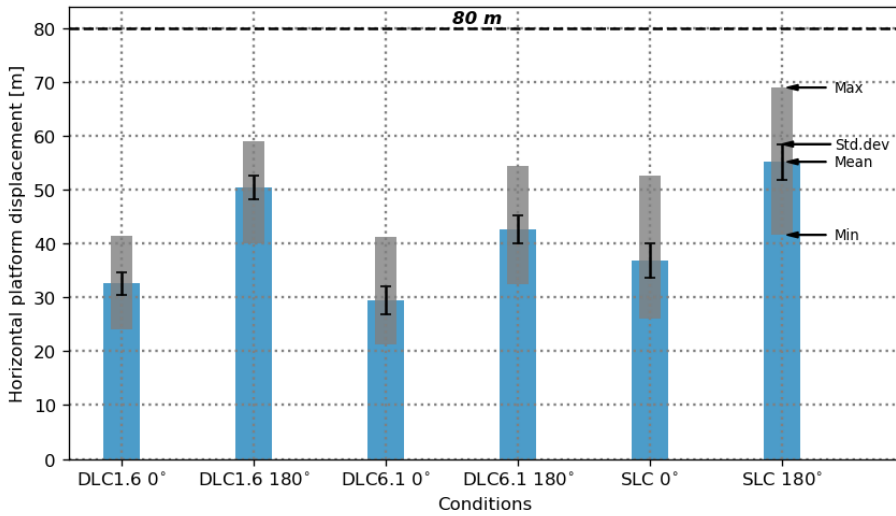


Figure 9. Statistics of the platform horizontal displacement

3.4.5 Fatigue Criteria

The fatigue analysis computes the mooring system’s lifetime fatigue damage across 100 binned metocean conditions representative of the Humboldt site [6]. The chain section is identified as the fatigue-limiting component in the mooring design; hence, in the subsequent analysis, only the results for the chain are presented.

The fatigue calculations follow ABS guidelines [8]. The fatigue damage is defined as the ratio of the number of load cycles experienced to the total number of cycles to failure for a particular tension range. Miner's summation rule is used to obtain the total damage over all tension ranges. The number of cycles to failure is obtained from T-N curves [8] for studless link chain with the slope parameter set to 3 and the intercept parameter set to 316. The number of load cycles experienced is calculated via rainflow counting using pCrunch⁴ v1.1.0. The fatigue damage contribution from each sea state is then weighted by the probability of occurrence of that sea state and summed over the 25-year lifetime to obtain the total accumulated damage.

Following [12], the MBL for the chain is adjusted to account for half the lifetime corrosion allowance (5 mm is half the lifetime corrosion allowance), reducing the MBL to 16,873 kN. To account for array wake effects, the wind speeds and the turbulence intensity for the fatigue bins are corrected as described in the design basis [1] (Section 6.4.2). The Jensen model [13],[14] is used to reduce the wind speed to account for wake deficit, and the Frandsen model [13] is used to increase the turbulence intensity to model the wake-added turbulence. Based on initial array layout design options, the inter-turbine spacing used for the correction is taken as 9.6D in all directions, where D is the diameter of the turbine rotor. The accumulated fatigue damage for different orientations of the platform for the three lines is indicated in Figure 10.

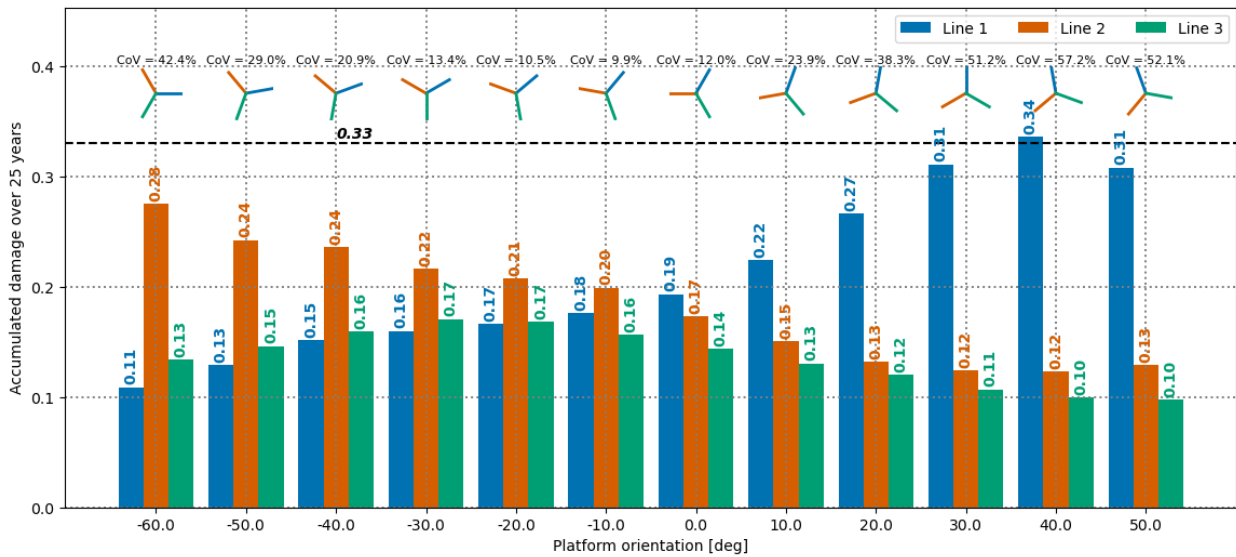


Figure 10. Accumulated fatigue damage for different platform orientations.

CoV = coefficient of variation

As observed from the wind rose in Figure 2, the Humboldt wind resource comes predominantly from the north-northwest direction. It is observed that the lines in each platform orientation that are close to this direction experience the largest fatigue damage. For instance, at the 40° orientation, which shows the largest damage, mooring line 1 is very close to the north direction; the least damage occurs in cases where two lines are approximately symmetrical around the north direction (for instance, orientation -30° and -20°). Based on the analysis, we conclude that

⁴ <https://github.com/NREL/pCrunch/releases/tag/v1.1.0>

the current chain sizing is sufficient to meet the fatigue requirement in all platform orientations except for a 40° platform heading, which should be avoided during the array design.

Furthermore, it is preferable to orient the platforms so that there is a near-uniform spread of fatigue damage over the three lines. This minimizes the overdesign of any one line, improving the efficiency of the mooring design. The coefficient of variation (CoV), calculated as the ratio of the standard deviation of damage to the mean value of the damage across the three lines, is indicated in Figure 10. Based on the CoV values for line fatigue damage, it is also preferred to avoid orientations 30°, 40°, 50°, and -60° in the array design, which have a CoV of line fatigue damage greater than 40%.

4 Anchor Design

Suction anchors were selected for the deep-water floating wind array because of their proven performance in taut and semi-taut mooring systems and their suitability for deep-water clay seabed types. Compared with drag or plate anchors, suction anchors provide higher load capacity, predictable installation, and precise positioning with minimal seabed disturbance. These characteristics make them an attractive solution for deep-water mooring systems where accurate alignment, installation reliability, and reduced environmental impact are critical.

The anchor was designed to meet the requirements of the taut mooring configuration described in Section 3, ensuring adequate load capacity under operational and extreme metocean conditions. The design was optimized following the methodology developed in earlier work [15], with final geometry and performance parameters selected to balance holding capacity, installability, and cost-effectiveness. Detailed optimization results and parametric analyses for this anchor design are documented in Lee et al. [16].

4.1 Design Assumptions and Requirements

The suction anchor design is based on soil conditions representative of the Humboldt reference site and the mooring loads found from the loads analyses discussed in Section 3. The seabed is assumed to consist of normally consolidated clay, with an undrained shear strength profile (s_u) defined as $s_u = 5 + 2z$ (kPa), where z is the depth below the seabed in meters [17]. The soil parameters were based on regional geological studies for the Humboldt wind energy area, as reported by the Bureau of Ocean Energy Management [17]. In addition, an adhesion factor was assumed in accordance with American Petroleum Institute (API) recommendations [18].

Anchor load demands were obtained from the taut mooring system described in Section 3. Coupled dynamic analyses were performed in OpenFAST under the three critical strength load cases: DLC 1.6, DLC 6.1, and SLC. Among the evaluated load cases, DLC 6.1 produced the highest line tensions and was used to govern the anchor sizing. For this case, safety factors of 2.4 for axial loading and 1.92 for lateral/inclined loading were applied in accordance with API RP 2SK [18] and ABS guidelines [8].

Each suction anchor was modeled as a vertical steel caisson installed by self-weight and suction underpressure. The mooring load was applied at a padeye located approximately two-thirds of the anchor length from the top, consistent with standard offshore design practice. The design verification considered combined vertical, horizontal, and inclined load components derived from the governing DLC 6.1 case.

Suction installability was evaluated following the approach of a previous study [15], using the ratio of critical to required underpressure (u_c/u_{up}) as a measure of installation safety. A minimum safety factor of 2.0 was targeted to ensure stable penetration and to prevent internal soil plug instability during suction installation.

4.2 Design Approach

The suction anchor design approach followed established offshore foundation design methodologies, focusing on load capacity, installation feasibility, and constructability. A range of aspect ratios ($L/D = 3-8$) was evaluated to determine the most effective configuration for the

taut mooring system. Each design option was assessed for its ability to resist the governing inclined mooring loads while maintaining practical fabrication and installation requirements.

The overall design workflow consisted of three main steps:

1. Load assessment – Mooring line loads at the padeye were obtained from coupled simulations in OpenFAST, as described in Section 3.
2. Capacity verification – Anchor capacity under axial, lateral, and inclined loads was checked using plastic limit analysis following the framework in earlier work [15],[16].
3. Installability evaluation – Suction penetration was analyzed using the ratio of allowable to required underpressure (u_c/u_{up}) to verify installation feasibility [15].

A minimum suction installation safety factor of 2.0 was targeted, in accordance with accepted industry practice for deep-water clay sites. Anchors with smaller aspect ratios ($L/D < 6$) typically demonstrated higher installation feasibility due to lower required underpressures, while longer, slender caissons ($L/D > 7$) required higher suction pressures and were less practical for field deployment.

Geotechnical efficiency, defined as the ratio of load capacity to anchor weight, was used as an auxiliary indicator of design performance. This metric allowed comparison between design alternatives to identify an optimal balance between holding capacity and material use. Although smaller anchors tended to yield higher efficiency, designs must also satisfy suction installability and fabrication constraints.

The optimization results showed that an aspect ratio around $L/D = 5$ provided the most favorable balance between load performance, material efficiency, and installation feasibility for the Humboldt site. This configuration was selected as the final reference design for subsequent verification and reporting.

4.3 Anchor Design Description

The final suction anchor configuration adopted for the reference array design was selected based on the results of the design screening described in Section 4.2. The governing load case was DLC 6.1, corresponding to a 50-year storm condition with a parked turbine. The anchor was designed to meet all strength and installation requirements under combined axial, lateral, and inclined loading.

The final design consists of a vertical suction caisson fabricated from steel with a dry unit weight of $7,850 \text{ kg/m}^3$. The mooring line is attached through a padeye positioned approximately two-thirds of the total anchor length from the top. The design ensures sufficient capacity to resist the maximum inclined load of 11.7 MN derived from mooring analysis, with adequate safety margins under both operational and survival conditions.

A summary of the key design parameters and verification results is provided in Table 8.

Table 8. Final Suction Anchor Configuration and Verification Summary

Parameter	Symbol and Units	Value
Governing design case	-	DLC 6.1
Water depth	-	800 m
Soil profile	-	NC clay ($s_u = 5 + 2z$ kPa)
Anchor type	-	Suction caisson
Diameter	D (m)	3.6
Length	L (m)	18.0
Padeye depth	-	$0.67L$ from the top
Inclined load demand	T_{max} (MN)	11.7
Capacity safety factor	-	>1.92 (inclined)
Suction installability safety factor	-	≈ 2.4
Steel mass	W (t)	~ 76

This configuration satisfies all design requirements for strength and suction installation feasibility. The chosen aspect ratio ($L/D = 5$) offers an optimal compromise between geotechnical capacity and installation practicality, while maintaining manageable fabrication weight and dimensions for offshore deployment.

4.4 Performance Results

The final suction anchor configuration was verified against applicable load cases using limit equilibrium and suction installation analyses. The design satisfies the geotechnical capacity, stability, and installation criteria defined in API RP 2SK [18] and ABS guidelines [8]. The results confirmed that the selected anchor dimensions ($D = 3.6$ m, $L = 18$ m) provide sufficient capacity to resist the governing inclined load of 11.7 MN with a safety factor greater than 1.92.

Suction installation analysis showed that the required underpressure during installation remains well below the critical limit, resulting in an installability ratio (u_c/u_{up}) of approximately 2.4. This ensures stable penetration without soil plug failure and confirms the feasibility of suction installation under the assumed soil conditions.

The chosen configuration also minimizes fabrication weight while maintaining acceptable stiffness and performance for the mooring layout. Compared with designs with larger aspect ratios, the selected geometry offers a practical compromise between holding capacity and ease of installation. The results align closely with the optimization trends reported in previous numerical studies [6], validating the applicability of the adopted design framework to deep-water conditions.

The design provides robust performance under the governing 50-year storm case (DLC 6.1) and remains within acceptable safety margins under the 500-year survival condition (SLC). The configuration established in this study serves as the reference design for future Task 49 deep-water array developments and potential design variants.

5 Dynamic Cable Design

The dynamic cable designs include both fully suspended and lazy-wave configurations. Fully suspended configurations can be cost effective for deep-water sites, as they may reduce the length of cable required. However, they present additional design challenges, as the response is coupled with the movement of adjacent wind turbines. Lazy-wave cables are also needed in places where the cable strings connect to the substation because the distance is too large for fully suspended cables. Additionally, lazy-wave cables offer more flexibility in routing, like to avoid mooring lines.

5.1 Design Assumptions and Requirements

The design assumptions and requirements for the dynamic cables were adapted from [1]. We designed dynamic cables for three conductor sizes to account for the necessary power transmission when multiple turbines are connected in strings. The conductor sizes are 300, 630, and 1,000 mm². The properties of the cable for each conductor size are shown in Table 9. For the buoyancy modules, we assumed a standard size of 1 m³ with the properties listed in Table 10.

Table 9. Dynamic Cable Properties

Parameter	Cable Type 1	Cable Type 2	Cable Type 3
Conductor size (mm ²)	300	630	1,000
Outer diameter (m)	0.161	0.184	0.203
Linear mass density (kg/m)	36.66	55.76	75.74
Axial stiffness (N)	469 x 10 ⁶	658 x 10 ⁶	854 x 10 ⁶
Bending stiffness (N·m ²)	19,920	42,470	68,729
Minimum breaking load (MBL) (kN)	383.2	537.4	698.4
Minimum bending radius (MBR) (m)	2.41	2.76	3.05

Table 10. Buoyancy Module Properties

Parameter	Value
Displaced volume (m ³)	1.0
Mass (kg)	480
Overall density (kg/m ³)	480
Length (m)	1.2
Diameter (m)	1.2

The critical design requirements for the dynamic cable are the maximum allowable tension and the minimum allowable bending radius. The maximum cable tensions are checked against the cable MBL, with a safety factor applied. The cable curvature is used to determine the bending radius, which is checked against the MBR, with a safety factor applied. Like the mooring and anchor designs, the cable designs were evaluated in critical load cases DLC 1.6, DLC 6.1, and

SLC. Based on the design basis, we targeted a safety factor of 2 for both tension and curvature in DLCs 1.6 and 6.1. In the SLC, we ensure that failure does not occur but accept a lower safety factor of 1.05. This is consistent with mooring tension safety factors in the DLCs and SLC. The MBL and MBR for each cable size are shown in Table 9.

5.2 Design Approach

The dynamic power cables were sized using a cable design optimization tool that varies the cable length, buoyancy section length, buoyancy section position, and buoyancy force, with the objective of minimizing cost while meeting design constraints. The optimization tool initially checks constraints on tension and curvature in the quasi-static model MoorPy [10]. The cable design optimization was repeated for each configuration (lazy-wave and suspended) and each conductor size. The larger conductor sizes are heavier and require more buoyancy force to offset the weight. After the initial design optimization, the dynamic cable designs were modeled in the lumped-mass mooring dynamics model MoorDyn to verify their dynamic performance [20]. MoorDyn modeling of cable bending stiffness is described and verified in [21].

A stand-alone MoorDyn driver model was used to isolate only the dynamic cable in time-domain simulations, with the platform motions and wave elevation time series inputted from previous OpenFAST simulations of the platform and mooring system. We used this approach to simplify the simulations and avoid fully coupled farm-level dynamics. Previous work has shown that the dynamic cable does not influence the motions of the platform [22], so this simplification is acceptable. For the suspended cable design, the platform motions of the adjacent turbines were modeled in two independent wind and wave realizations. Again, this is a conservative assumption intended to elicit maximum tensions from the suspended cable design. For the OpenFAST simulations of the platform and mooring system, we used OpenFAST version 3.5.2 [23]. Only a single seed was considered for the wave-wind realizations and safety factors were calculated using the maximum tension or curvature seen in that simulation. Future work should consider additional seeds and potentially apply the Gumbel distribution fit to determine the most probable maximums.

In all cases, we assumed aligned wind, wave, and current loading to be conservative. We selected only the critical environmental headings to reduce the number of necessary simulations. The lazy-wave cable designs were simulated in DLC 1.6, DLC 6.1, and SLC at 0° and 180° headings, where the 180° heading is expected to produce maximum curvature and 0° heading is expected to produce maximum tensions. For the suspended cable, preliminary work showed that the cable tensions were at a maximum when the environmental loading was perpendicular to the cable direction, so only the 90° heading was evaluated. Throughout the wind farm, the mooring system orientation relative to the cable may vary. To be conservative, the maximum platform offsets in a given load case are assumed for all heading directions. This ensures the cable's safety in every load case for any mooring orientation. The considered environmental heading directions for the lazy-wave and suspended cable designs are shown in Figure 11.

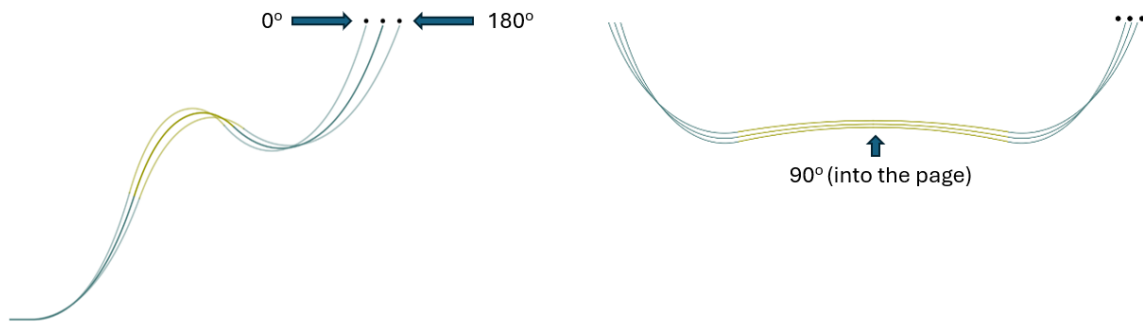


Figure 11. Driving environmental loading directions used in dynamic cable simulations

5.3 Suspended Cable Design Descriptions

The suspended power cables are headed along turbine rows that run roughly east to west. The spacing is 1,526.4 m between turbines, and the cables are assumed to attach on the outside of the center column at a 5-m radius from the turbine center. The resulting span of the suspended power cables is 1,516.4 m. The cable length and buoyancy force were optimized to meet constraints on the allowable tension and cable curvature, which were evaluated during design load cases. The cable tension was the driving design constraint, especially due to the weight of marine growth and the extreme current loading. To mitigate the impacts of marine growth on the cable tensions, the midpoint of the cable was kept below 170 m, based on the assumptions in Table 4.

The optimized cable profiles are shown in Figure 12 and defined in Table 11 for the three conductor sizes. The 300-mm² conductor size was the most challenged by tension because the MBL is lowest. To mitigate against the current loading and resulting high tensions, this design has a longer cable length of 1,851 m and sits lower in the water column. This reduces the current loading because the current speed decays with depth. The larger conductor sizes of 630 and 1,000 mm² did not require this modification, and have a shorter cable length of around 1,700 m. All designs have a fixed buoyancy section length of 800 m, and the number of buoyancy modules varies at 25, 46, and 70 for the 300-, 630-, and 1,000-mm² conductor sizes, respectively. The larger conductor sizes required more buoyancy modules because the cable weight is greater.

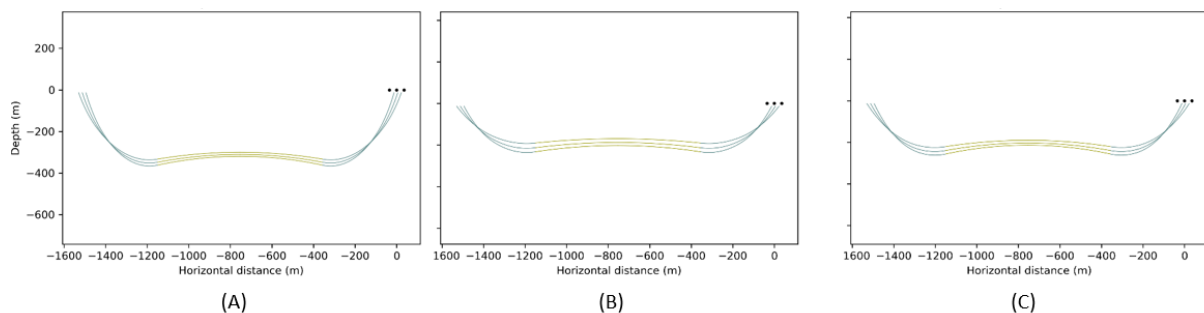


Figure 12. Suspended cable profiles for conductor sizes of (a) 300-mm², (b) 630-mm², and (c) 1,000-mm² conductor sizes

Table 11. Suspended Cable Design Parameters

Conductor Size (mm²)	300	630	1,000
Span (m)	1,516.4	1,516.4	1,516.4
Total cable length (m)	1,851.33	1,670.99	1,703.70
Length of cable above buoyancy section	525.67	435.50	451.85
Buoyancy section length (m)	800	800	800
Number of buoyancy modules	25	46	70
Buoyancy module spacing (m)	33.18	17.76	11.59
Averaged diameter of buoyancy section (m)	0.26	0.33	0.39
Averaged mass of buoyancy section (kg/m)	51.73	83.38	117.77

Marine growth was applied to the suspended cable designs following the assumptions in Table 4. The cables were designed so that the upmost point of the buoyancy section (sometimes called the hog point) stayed below the marine growth threshold of 170 m, so marine growth was added to the cable attachments at either platform. Based on the profile, 100 mm of marine growth was added to the upper approximately 40 m of cable on either side, and 50 mm of marine growth was added to the next 140–180 m of cable, depending on the design. The length of cable to add marine growth to was calculated using the quasi-static model MoorPy [10]. The length and properties of the cable with added marine growth are shown in Table 12.

Table 12. Suspended Cable Parameters With Marine Growth

Conductor Size (mm²)	300	630	1,000
Length of cable with 100 mm of marine growth (m)	40.06	42.01	40.99
Averaged diameter of cable with 100 mm of marine growth (m)	0.36	0.38	0.40
Averaged mass of cable with 100 mm of marine growth (kg/m)	145.17	173.98	202.11
Length of cable with 50 mm of marine growth (m)	143.04	184.97	169.21
Averaged diameter of cable with 50 mm of marine growth (m)	0.26	0.28	0.30
Averaged mass of cable with 50 mm of marine growth (kg/m)	80.51	104.46	128.52

5.4 Lazy-Wave Cable Design Descriptions

Lazy-wave cables are used in some places within the farm to connect strings back to the substation or to avoid interference with mooring lines. The initial lazy-wave cable design was based on previous work [22]. However, the cable design was challenged by strong currents that exerted large loads on the cable. To mitigate this, the touchdown point was extended to 1,000 m, creating a more elongated design that can better handle the current loading. The lazy-wave cable profile is shown in Figure 13.

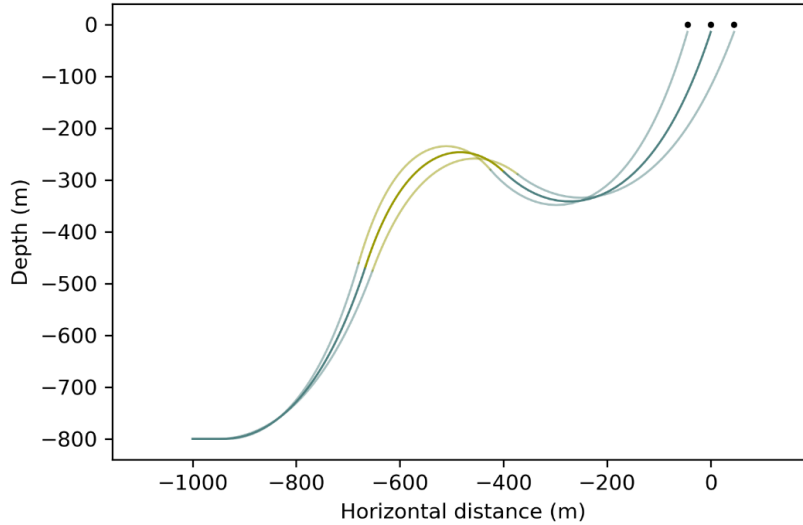


Figure 13. Lazy-wave cable profile at 0 m, -45 m, and 45 m offsets

The lazy-wave cable design parameters are shown in Table 13 for the three conductor sizes of 300, 630, and 1,000 mm². The cable length is 1,512 m over a span of 1,000 m for all three conductor sizes. The buoyancy section length is fixed at 400 m. The number of buoyancy modules increases for the larger conductor sizes to offset the increased weight of the cable. The number of buoyancy modules is 29, 52, and 78 for the 300-, 630-, and 1,000-mm² conductor sizes, respectively.

Table 13. Lazy-Wave Cable Design Parameters

Conductor Size (mm²)	300	630	1,000
Span (m)	1,000	1,000	1,000
Total cable length (m)	1,511.71	1,511.71	1,511.71
Length of cable below buoyancy section (m)	516.87	516.87	516.87
Buoyancy section length (m)	400	400	400
Length of cable above buoyancy section (m)	594.84	594.84	594.84
Number of buoyancy modules	29	52	78
Buoyancy module spacing (m)	14.32	7.8	5.21
Averaged diameter of buoyancy section (m)	0.34	0.45	0.54
Averaged mass of buoyancy section (kg/m)	71.37	118.50	169.04

The lazy-wave cables were also modeled with marine growth based on the assumptions in Table 4; 100 mm of marine growth was applied to the upper 41 m of cable, and 50 mm of marine growth to the next 137 m of cable. The rest of the cable, including the buoyancy section, stayed below the 170-m depth threshold and remained the same. The cable properties with the added marine growth are shown in Table 14. The lazy-wave cable design tensions and curvature were verified with marine growth added to ensure performance.

Table 14. Lazy-Wave Cable Parameters With Marine Growth

Conductor Size (mm ²)	300	630	1,000
Length of cable with 100 mm of marine growth	41.20	41.24	41.23
Averaged diameter of cable with 100 mm of marine growth (m)	0.36	0.38	0.40
Averaged mass of cable with 100 mm of marine growth (kg/m)	145.17	173.98	202.11
Length of cable with 50 mm of marine growth (m)	137.38	137.73	137.74
Averaged diameter of cable with 50 mm of marine growth (m)	0.26	0.28	0.30
Averaged mass of cable with 50 mm of marine growth (kg/m)	80.51	104.46	128.52

5.5 Performance Results

The dynamic cable designs were evaluated in select critical load cases to ensure their safety and performance. For each load case, a single realization was simulated for 4,200 s, with the first 600 s removed for transient dissipation. The maximum tensions and curvature in each simulation were used to calculate the safety factors.

5.5.1 Maximum Tensions

The suspended cable tension statistics in a 90° environmental heading are shown in Figure 14. Using the design basis, we targeted a safety factor of 2 for the cable tensions and curvature. For all three designs, the maximum cable tensions have a safety factor of greater than 2 in DLCs 1.6 and 6.1 but less than 2 in the SLC. This was deemed acceptable because the tensions stay below the MBL, and the SLC has a very low 500-year return period. The tensions are highest for the 1,000-mm² cable, likely because it is the heaviest.

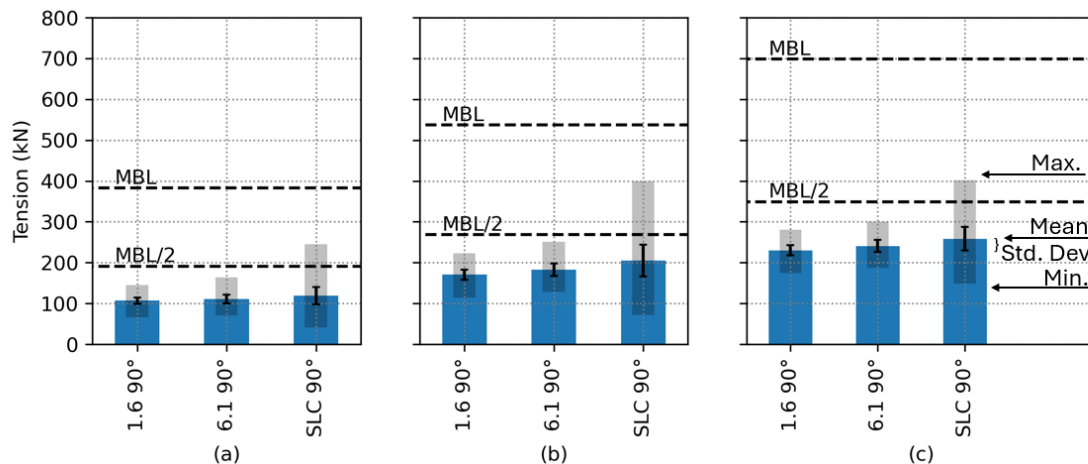


Figure 14. Suspended cable tensions for (a) 300-mm², (b) 630-mm², and (c) 1,000-mm² conductor sizes

The lazy-wave cable tension statistics are displayed in Figure 15 for both 0° and 180° environmental headings. For all three conductor sizes, the cable tensions stay below the MBL divided by a safety factor of 2. The cable tensions are slightly higher in the 0° loading direction, because the platform is offsetting away from the cable touchdown point, extending the cable. Again, the 1,000-mm² cable has the largest tensions. The tensions are largest in the SLC case, but there is no significant variation across the different cases.

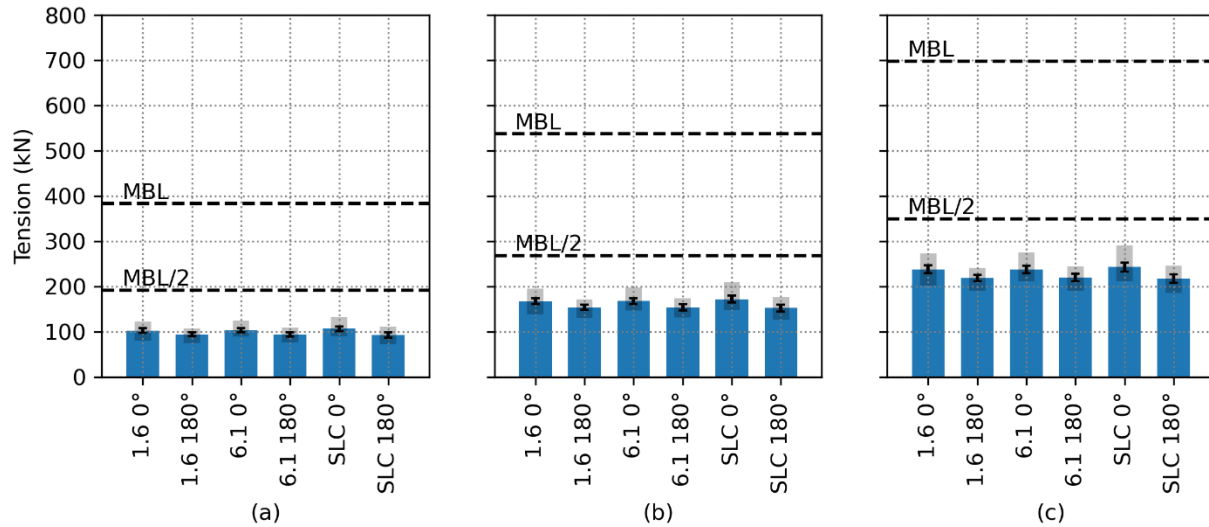


Figure 15. Lazy-wave cable tensions for (a) 300-mm², (b) 630-mm², and (c) 1,000-mm² conductor sizes

5.5.2 Maximum Curvature

The maximum curvature for the suspended cable designs is shown in Figure 16 for a 90° environmental heading. In all three designs, the curvature is well below the inverse of the MBR with a safety factor of 2 applied. The curvature is highest in the SLC case due to the large current speed. The curvature is lowest for the 1,000-mm² design, likely because the cable is the heaviest and the shape is the least impacted by the current loading.

The suspended cable curvature along the arc length is shown in Figure 17 for the worst case (SLC at a 90° heading). The cable curvature is largest at either end of the cable, where it connects to the platforms.

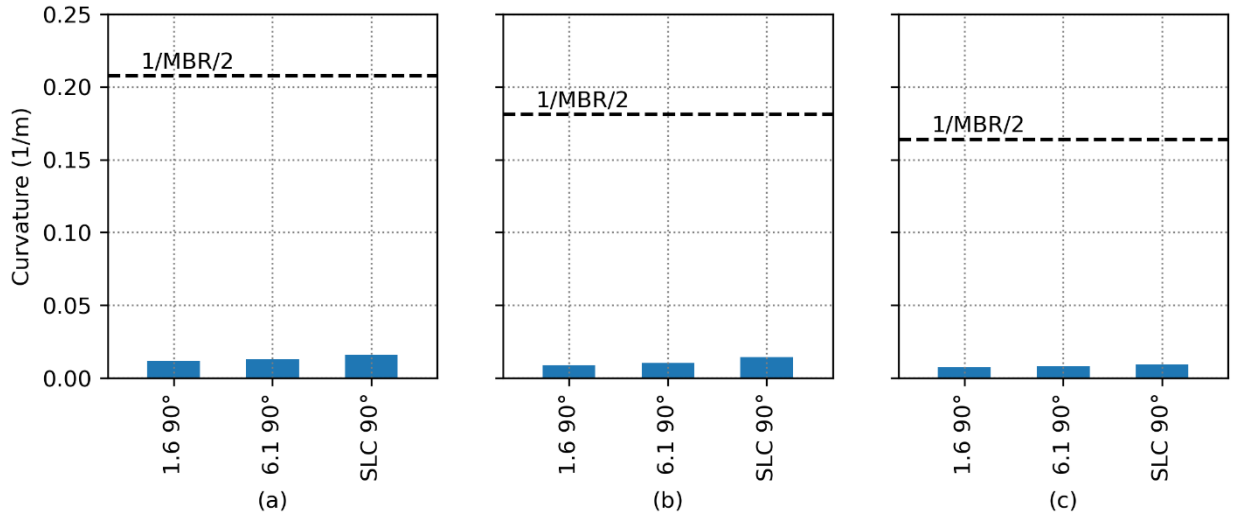


Figure 16. Suspended cable maximum curvature for (a) 300-mm², (b) 630-mm², and (c) 1,000-mm² conductor sizes

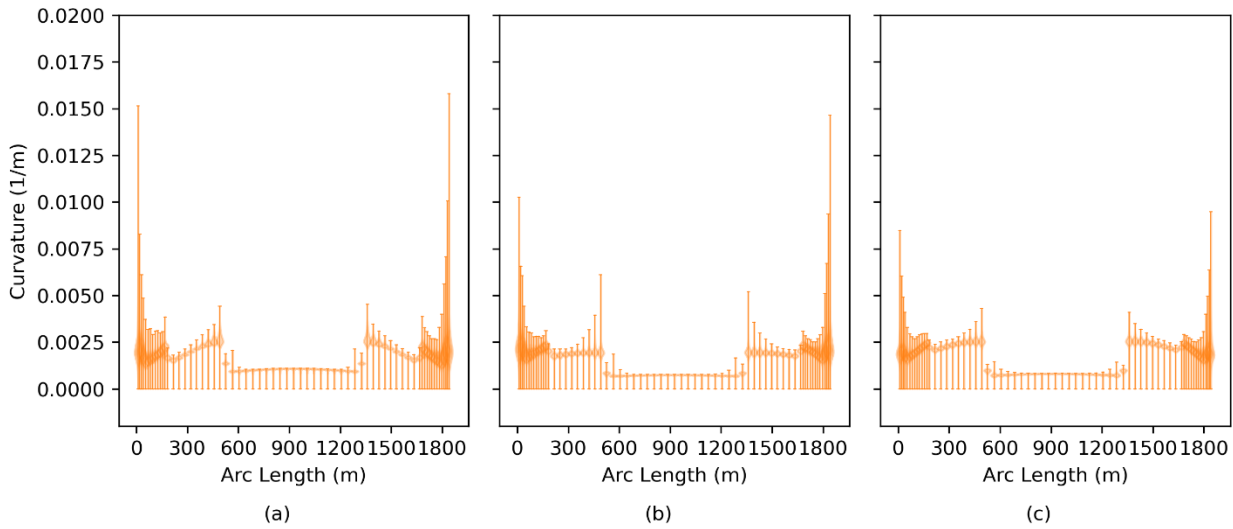


Figure 17. Violin plots of suspended cable curvature in SLC 90° for (a) 300-mm², (b) 630-mm², and (c) 1,000-mm² conductor sizes

The maximum curvature for the lazy-wave cable designs is shown in Figure 18 for the 0° and 180° environmental headings. Like the suspended cable results, the lazy-wave curvature is well below the inverse of the MBR with a safety factor of 2 applied. In every case, the curvature is higher for the 180° heading. This heading points directly toward the cable’s touchdown point, compressing the lazy-wave shape and increasing the curvature. The curvature is again highest for the 300-mm² conductor size, which is the lightest and most impacted by the current loading.

The lazy-wave cable curvature along the arclength is shown in Figure 19 for the SLC at a 180° heading, which is the case with the highest curvature. The curvature is highest at approximately 50-m arclength, which is where the cable lifts off of the seabed.

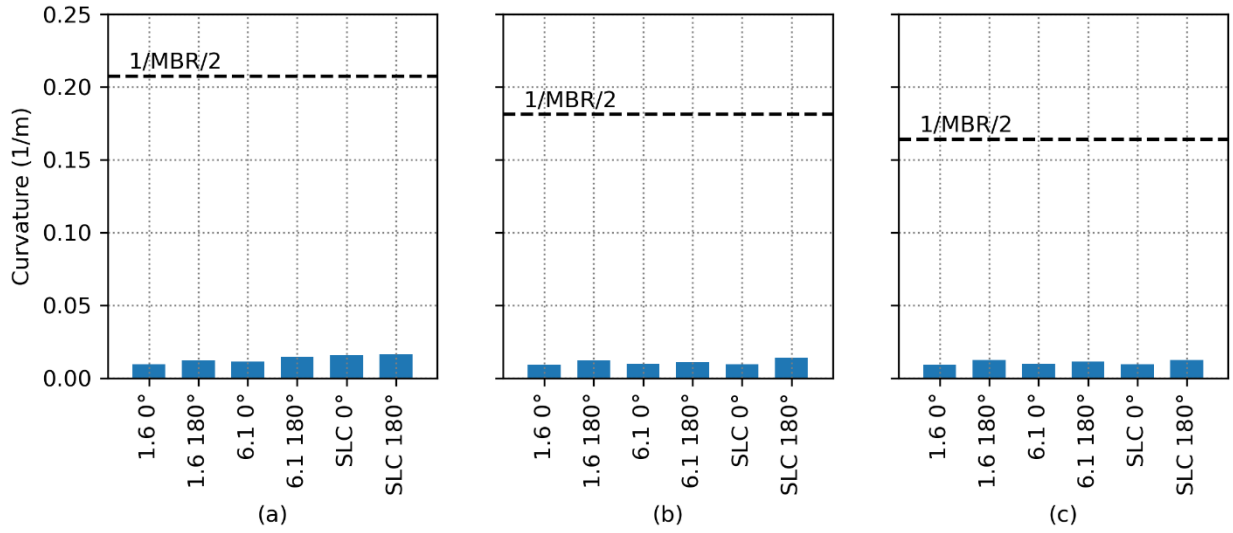


Figure 18. Lazy-wave maximum curvature for (a) 300-mm², (b) 630-mm², and (c) 1,000-mm² conductor sizes

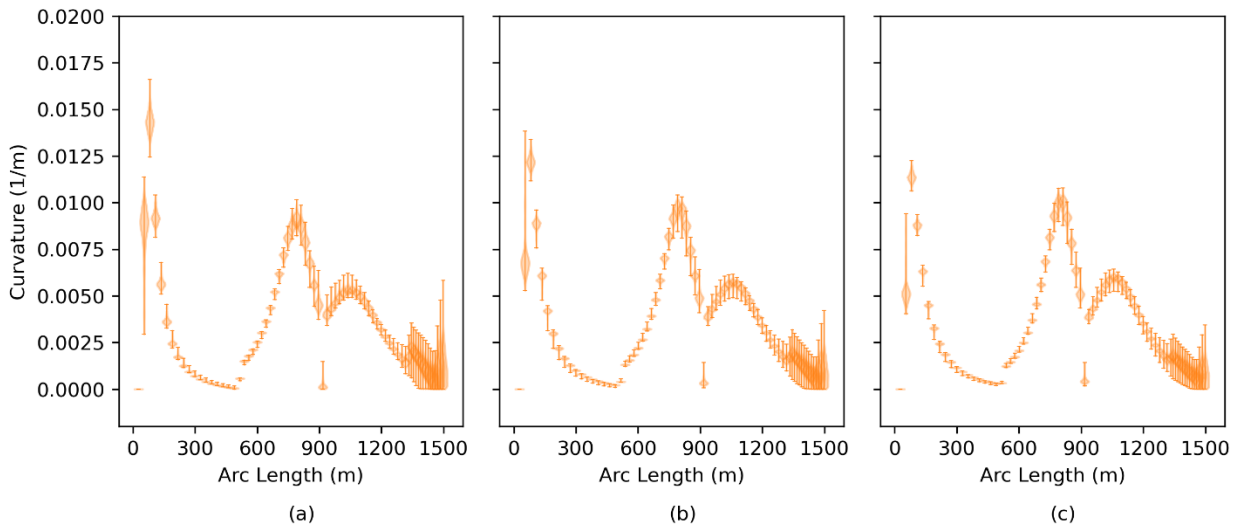


Figure 19. Violin plots of lazy-wave cable curvature in SLC 180° for (a) 300-mm², (b) 630-mm², and (c) 1,000-mm² conductor sizes

6 Layout

The array layout was constrained to use regular grid spacing, based on the initial design scoping described in Table 1. For the boundaries of the farm, a square-shaped region was assumed with an area of 256 km², matching the size of the Humboldt northeast lease area. These assumptions were intended to produce a more generic and broadly useful array design, instead of designing for a specific lease area.

The layout of the floating wind farm must consider spatial constraints that prevent clashing or collision with adjacent components. These constraints include a minimum distance between turbines and minimum clearance between the mooring lines. Also, the mooring lines must not extend beyond the boundaries of the lease area. These specific constraints are described in the design basis [1]. Additional constraints related to power cables are accounted for when the power cables are routed, after a layout is defined.

In practice, spatial constraints are modeled as two-dimensional buffer zones that cannot overlap to ensure sufficient clearances between turbines, moorings, and boundaries, as shown in Figure 20.

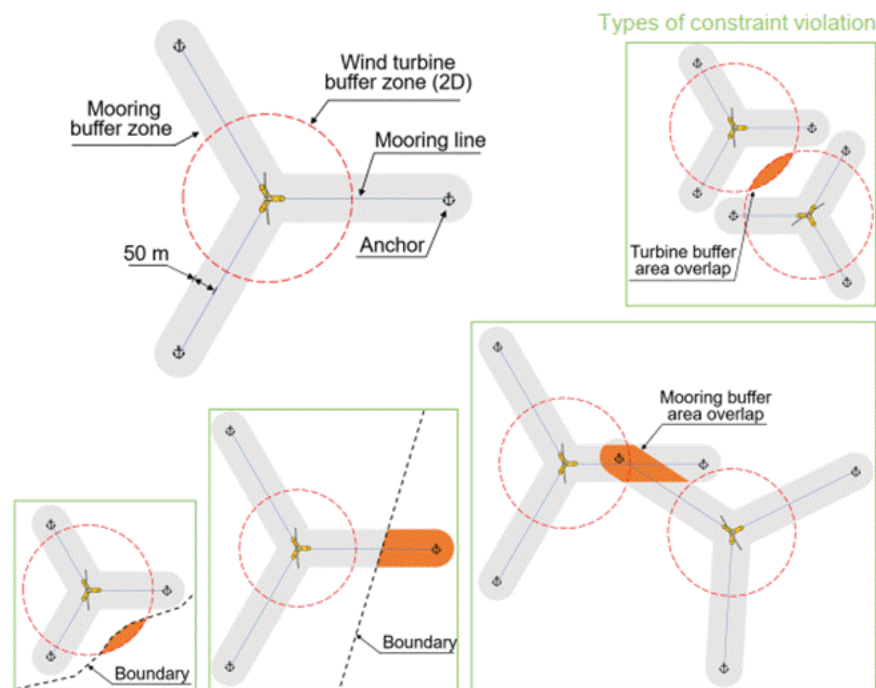


Figure 20. Spatial constraints around mooring lines and platforms for layout optimization [24]

Additionally, a regular grid layout of the wind turbine positions has been assumed, which is the most common choice for navigation purposes. The full parameterization of a regular, gridded layout is described in the design basis [1] and summarized in Figure 21.

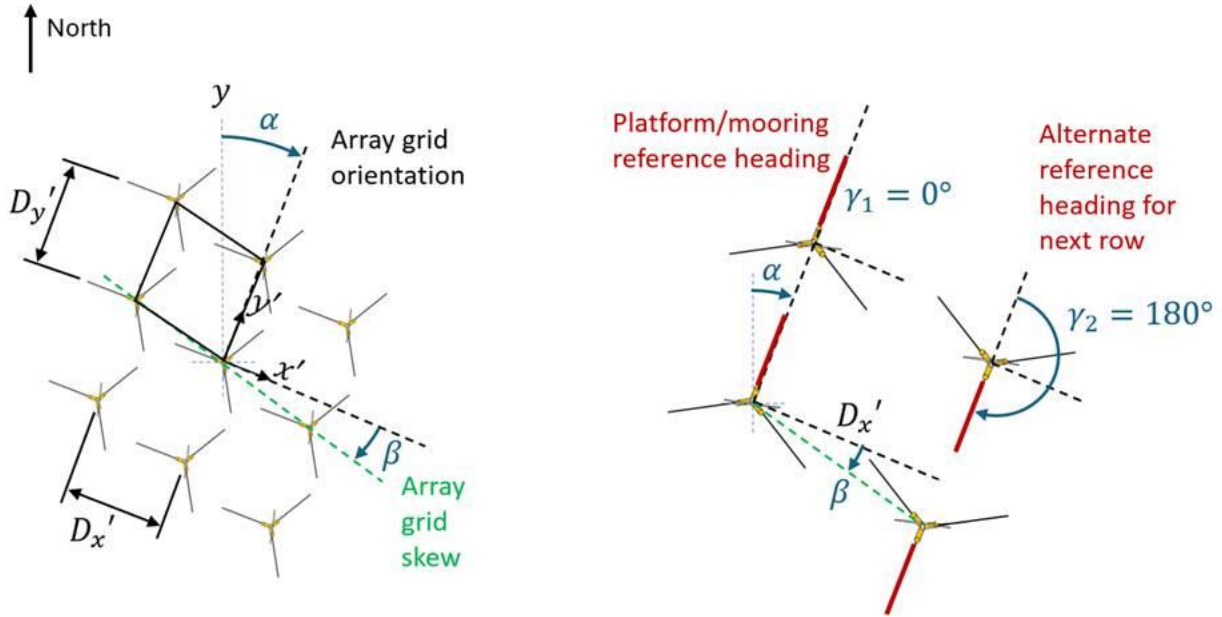


Figure 21. Parameterization of regular, gridded array layout [1]

The layout optimization problem, constraints, parameterization, and solving algorithm are presented in [25]. The methodology is based on the construction of a regular, gridded pattern for the turbine positions and consists of two steps. First, the turbine positions are placed within the lease area with the goal of maximizing the annual energy production (AEP). Second, the mooring line orientations are selected.

In the first step, the optimization objective is to minimize wake losses within the array, subject to the regular layout approach and spatial constraints. The regular layout approach implies that the turbines are positioned within a regular grid composed of parallelograms (as pictured in Figure 21), whose shape and orientation are a function of the design variables. Dx' and Dy' are the distances between turbines along the two directions of the grid, α defines the orientation of the grid according to the north and β defines the array grid skew (deformation of the parallelogram).

In the second step, we developed two variations of the algorithm: the first maximizes the distance between mooring lines and the second minimizes the interaction between mooring line orientations and environmental loading. This report presents only the results obtained with the second variation, which minimizes fatigue damage to the mooring line considering the environmental loading directions. The mooring system heading is defined by γ .

The Humboldt wind resource, as shown in Figure 2, features wind predominantly from the north and northwest. Thus, the priority was to increase turbine spacing in the predominant wind direction to decrease wake losses. The decrease in wake losses is beneficial for the farm's AEP and for minimizing mooring fatigue damage, which increases with increased turbulence intensity due to wake effects. For the mooring system, it is also beneficial to avoid heading the mooring lines in the predominant wind direction to minimize fatigue loading.

The final selected layout has turbine spacings of $Dx' = 1,526.4$ m and $Dy' = 1,701.6$ m, without array grid skew ($\beta = 0$). The columns are oriented at 20° , rotating clockwise from due north. This layout limits the wake losses to 4.56%. Concerning mooring lines, headings of $\gamma = 0^\circ$ and $\gamma = 180^\circ$ were selected for alternating columns. These alternating mooring system orientations allow the turbine columns to slot more closely together, which is necessary to fit 67 turbines within the lease area. Additionally, the selected mooring orientations avoid heading a mooring line in the due north direction, which reduces fatigue damage.

The parameters of the final array layout and mooring line orientation are summarized in Table 15.

Table 15. Array Layout and Mooring Line Orientation Parameters

Parameter	Value
Turbine spacing Dx' (m)	1,526.4
Turbine spacing Dy' (m)	1,701.6
Grid rotation α ($^\circ$)	20
Array grid skew β ($^\circ$)	0
Mooring line heading first row γ_1 ($^\circ$)	0
Mooring line heading next row γ_2 ($^\circ$)	180

The array layout, cable routing, and mooring orientations are shown in Figure 22. The substation location was selected to fit within the regular, gridded layout of the array, based on U.S. Coast Guard recommendations. The substation is located on the east side of the array, which is closer to shore for the Humboldt region and minimizes the length of the export cable.

The cable routing was performed manually, with each row roughly grouped together as a cluster. The top and bottom clusters include the turbines in the far corner. The cable routing includes cables of conductor sizes 300, 630, and $1,000 \text{ mm}^2$, based on the available cable designs. The chosen cable for each turbine connection is a function of the number of turbines connected in a string. The cables that connect turbines from the northwest to southeast are fully suspended over the 1,526.4-m turbine spacing. At the northeast and southwest corners, there are lazy-wave connections, angled in a triangle. This was chosen to ensure that the cables avoid the mooring lines. At the end of each cluster before the substation connection, there is a lazy-wave cable that connects to static cable. The static cable routes along the seafloor, avoiding anchors, before connecting to the substation. The substation design and detailed cable connections at the substation are out of scope for this study.

Figure 23 shows a three-dimensional view of the array with the combination of suspended and lazy-wave cables. The turbine and substation coordinates are listed in Table 16.

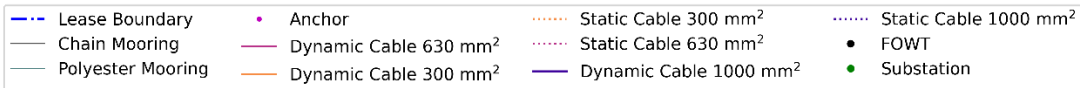
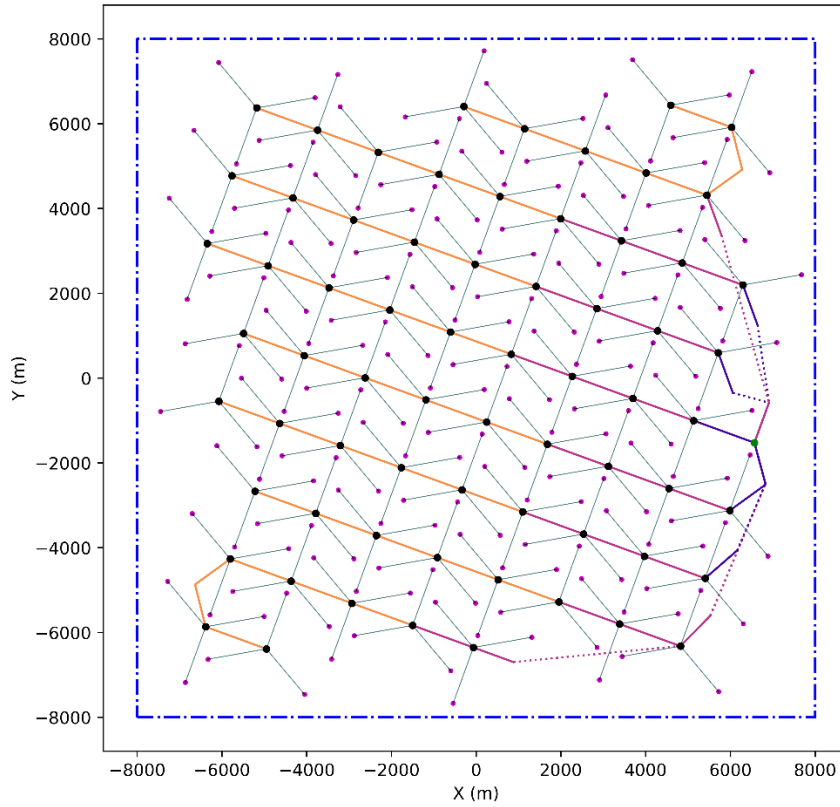


Figure 22. Array layout and cable routing

FOWT = floating offshore wind turbine

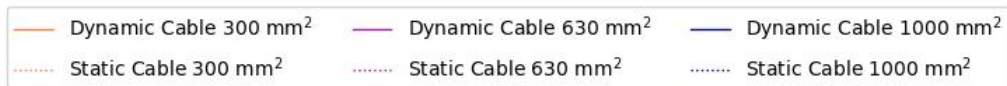
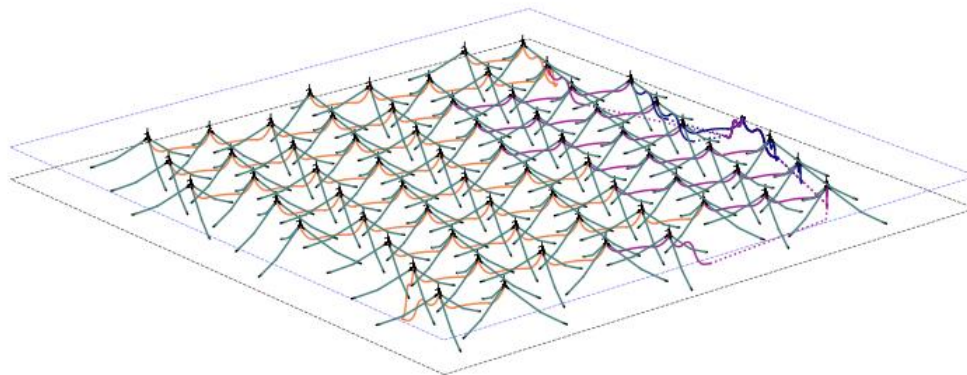


Figure 23. Three-dimensional view of the deep-water array design

Table 16. Turbine and Substation Coordinates

Substation/ Turbine No.	Platform x (m)	Platform y (m)	Substation/ Turbine No.	Platform x (m)	Platform y (m)
Substation	6,568.7	-1,525.84	Turbine 34	2,577.2	5,359.3
Turbine 1	4,822.7	-6,322.78	Turbine 35	-2,930.99	-5,311.46
Turbine 2	5,404.7	-4,723.8	Turbine 36	-2,349.01	-3,712.48
Turbine 3	5,986.7	-3,124.82	Turbine 37	-1,767.02	-2,113.5
Turbine 4	3,388.4	-5,800.72	Turbine 38	-1,185.04	-514.52
Turbine 5	3,970.4	-4,201.74	Turbine 39	-603.06	1,084.46
Turbine 6	4,552.3	-2,602.76	Turbine 40	-21.08	2,683.4
Turbine 7	5,134.3	-1,003.78	Turbine 41	560.9	4282.4
Turbine 8	5,716.3	595.2	Turbine 42	1,142.88	5,881.4
Turbine 9	6,298.3	2,194.2	Turbine 43	-4,947.32	-6,388.39
Turbine 10	1,954.03	-5,278.66	Turbine 44	-4,365.33	-4,789.4
Turbine 11	2,536	-3,679.68	Turbine 45	-3,783.35	-3,190.42
Turbine 12	3,118	-2,080.7	Turbine 46	-3,201.37	-1,591.44
Turbine 13	3,700	-481.72	Turbine 47	-2,619.39	7.54
Turbine 14	4,282	1,117.26	Turbine 48	-2,037.41	1,606.52
Turbine 15	4,863.9	2,716.2	Turbine 49	-1,455.43	3,205.5
Turbine 16	5,445.9	4,315.2	Turbine 50	-873.45	4,804.5
Turbine 17	6,027.9	5,914.2	Turbine 51	-291.46	6,403.5
Turbine 18	-62.29	-6,355.58	Turbine 52	-6,381.66	-5,866.33
Turbine 19	519.69	-4,756.6	Turbine 53	-5,799.68	-4,267.34
Turbine 20	1,101.67	-3,157.62	Turbine 54	-5,217.7	-2,668.36
Turbine 21	1,683.65	-1,558.64	Turbine 55	-4,635.72	-1,069.38
Turbine 22	2,265.6	40.34	Turbine 56	-4,053.74	529.6
Turbine 23	2,847.6	1,639.32	Turbine 57	-3,471.76	2,128.6
Turbine 24	3,429.6	3,238.3	Turbine 58	-2,889.77	3,727.6
Turbine 25	4,011.6	4,837.3	Turbine 59	-2,307.79	5,326.5
Turbine 26	4,593.6	6,436.3	Turbine 60	-6,070.07	-547.32
Turbine 27	-1,496.64	-5,833.52	Turbine 61	-5,488.08	1,051.66
Turbine 28	-914.66	-4,234.54	Turbine 62	-4,906.1	2,650.6
Turbine 29	-332.68	-2,635.56	Turbine 63	-4,324.12	4,249.6
Turbine 30	249.3	-1,036.58	Turbine 64	-3,742.14	5,848.6
Turbine 31	831.28	562.4	Turbine 65	-6,340.45	3,172.7

Turbine 32	1,413.27	2,161.4	Turbine 66	-5,758.47	4,771.7
Turbine 33	1,995.25	3,760.4	Turbine 67	-5,176.49	6,370.7

7 Cost and Logistics Modeling

This section outlines the methodology, assumptions, and results for assessing the costs, logistics, and energy production of the reference array design. Using simulation models selected from the design basis—including process-based models for installation and operations and maintenance (O&M) logistics, as well as a wake and AEP model—we estimate capital expenditures (CapEx), operational expenditures (OpEx), net AEP, and levelized cost of energy (LCOE) [1]. The subsections that follow describe the modeling approach; outline key assumptions regarding plant design, site conditions, and financial and operational parameters; and present the resulting cost and performance estimates. This structured methodology provides a robust framework for comparing alternative wind farm designs and supporting research and collaboration aimed at reducing the cost of energy.

7.1 Methodology

The LCOE is calculated as:

$$LCOE = \frac{FCR \times CapEx + OpEx}{net\ AEP} \quad (1)$$

where FCR is the fixed charge rate, a metric used to annualize CapEx while accounting for financing assumptions such as cost of debt, cost of equity, and project leverage [26]. CapEx represents the initial investment costs for project development, including the cost categories outlined in the National Laboratory of the Rockies' (NLR's) *Cost of Wind Energy Review* [27]. This covers investment costs from generation up to the point of interconnection (POI). OpEx covers ongoing operational expenditures, following the same cost categories as in [27]. Net AEP is calculated accounting for internal wake losses, electrical losses, technical losses, environmental losses, and availability losses. All these metrics are estimated using the open-source simulation models described below under the “Modeling Tools” heading.

For this analysis, the LCOE was calculated using the FCR approach rather than the discounted cash flow method outlined in the design basis [1], which accounts for the timing of investments, loan payments, interest, OpEx, decommissioning costs, and salvage revenue. While the design basis provides sufficient information to calculate the weighted average cost of capital (WACC), it does not specify key timing parameters such as loan tenor or repayment structure (e.g., mortgage-style, linear). The FCR approach avoids these requirements while still producing an annualized cost metric. To remain consistent with the design basis objective of producing comparable LCOE estimates across different designs and regions, the FCR was calculated on a pre-tax basis with a 100% net present value adjustment for depreciation (no adjustment for depreciation).

Four open-source modeling tools from NLR were used for this analysis:

- Offshore Renewables Balance-of-System and Installation Tool (ORBIT): balance of system (BOS) and installation costs and logistics
- Windfarm Operations and Maintenance cost-Benefit Analysis Tool (WOMBAT): O&M costs, wind farm availability, and logistics
- FLOW Redirection and Induction in Steady State (FLORIS): AEP and wake losses

- Wind Asset Value Estimation System (WAVES): integrates the three models above to calculate the LCOE.

ORBIT provides medium-fidelity modeling of offshore installation logistics and associated costs through a discrete-event simulation framework that accounts for weather-related delays [28]. Component sizing and costs are derived either from built-in engineering design modules or user inputs. The cost database within ORBIT is maintained by NLR and is regularly updated to reflect current industry and market trends. Using ORBIT, we estimate the CapEx for the reference wind plant.

WOMBAT is a scenario-based O&M modeling tool that simulates the costs associated with component failures, scheduled and unscheduled maintenance, and equipment mobilization within a discrete-event simulation environment [29]. Rather than optimizing O&M strategies, WOMBAT quantifies the effects of new technologies, maintenance approaches, and site conditions on the operational performance and cost of wind farms. With WOMBAT, we estimate the OpEx and production-based availability, which is later used to determine the net AEP.

FLORIS is a steady-state wind farm performance model designed to evaluate wake effects and optimize turbine control strategies. Implemented in Python, FLORIS uses engineering wake models to estimate energy production and wake losses under specified wind farm layouts and site conditions [30].

WAVES integrates results from the three models—CapEx from ORBIT, OpEx and availability from WOMBAT, and AEP from FLORIS—along with financial assumptions and other loss parameters to estimate the LCOE for both wind farms [31].

7.2 Assumptions

This subsection summarizes the key assumptions used in the analysis. It is important to note that ORBIT, WOMBAT, FLORIS, and WAVES each include numerous built-in assumptions within their default configuration files, default input parameters, and model installation and maintenance logistics processes. As such, this report does not explicitly document all underlying model defaults; instead, it highlights only the assumptions that deviate from the models' default settings.

For additional details on model assumptions, refer to the project library⁵ containing the configuration files used to generate the Task 49 Deep-Water Array Design results. These simulations were conducted using ORBIT version 1.2.4,⁶ WOMBAT version 0.12.2, FLORIS version 4.5.1, and WAVES version 0.6.1.

⁵ <https://github.com/dmulash/WAVES/tree/analysis/iea-task-49-deep-design/library/iea-task-49-deep-design> Jupyter notebook at <https://github.com/dmulash/WAVES/blob/analysis/iea-task-49-deep-design/examples/iea-task-49-deep-design-notebook.ipynb>

⁶ Technically the dev branch of ORBIT as of November 13, 2025, which has some unreleased features ahead of version 1.2.4. If released by time of publication, we recommend using version 1.2.5. to be able to replicate the results.

7.2.1 Plant Characteristics Summary

For this design variant, the cost and logistics models explicitly simulate installation activities and associated costs under site-specific conditions representative of the Humboldt deep-water location (~800 m). Costs and masses for the mooring system (taut lines with suction pile anchors) and intra-array cable system were not independently derived within the models; instead, they were precalculated based on the design characteristics described earlier in this report and incorporated directly as procurement cost inputs. Additional details on these component costs and masses are provided in Section 7.2.2.

To model the export system costs and the installation and O&M logistics of this reference plant, assumptions were made regarding the distances between the offshore substation and the POI, as well as between the wind farm and the installation and O&M port. For this analysis, Zone 1 (Elk River) was selected as the POI. This study does not include a comprehensive evaluation of all possible POI locations; rather, it adopts a representative site within Zone 1 based on the Substation Evaluation conducted by the California Energy Commission for the Humboldt Wind Energy Area [32].

From a modeling standpoint, the Port of Humboldt Bay was designated as both the construction and O&M port due to its proximity to the selected site. Phase 1 of this port development is planned to encompass approximately 98 acres, with potential for future expansion. While no formal announcement has been made regarding construction or commissioning timelines, this analysis assumes that the port is fully operational and equipped to support both the installation and long-term maintenance of the reference wind farm [33].

Figure 24 illustrates the reference site within the Humboldt lease areas OCS-P 0561 and OCS-P 0562, along with the assumed transmission and logistics routes used to determine relevant distances for cost modeling.

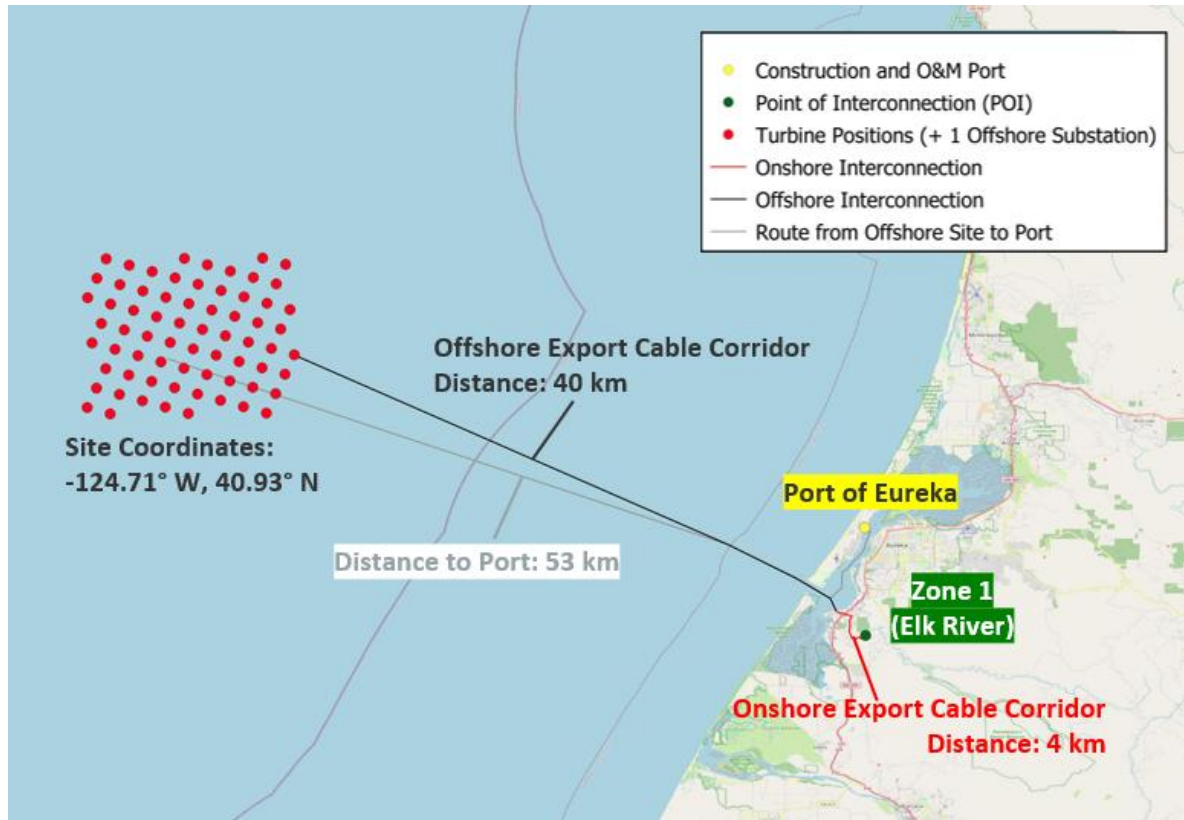


Figure 24. Reference site located within the Humboldt lease areas (OCS-P 0561 and OCS-P 0562), showing assumed routes and calculated distances used for cost and logistics modeling

Weather data from [4] and [5] were initially considered for use in the simulations; however, missing values were identified in the wave height data, which could compromise the accuracy of installation and O&M logistics simulations in ORBIT and WOMBAT. To address this issue, ERA5⁷ reanalysis wind speed and wave height data (1989–2019) were used as input for simulations [34]. Installation was assumed to begin in 1998, and operations (generation and O&M) were modeled with data from 1999 through 2018, providing 20 years of operational data for the analysis.

7.2.2 Task 49 Design Basis Cost and Logistics Considerations

Several recommendations and considerations from the Task 49 design basis cost and logistics guidance [1] were incorporated into this analysis. Table 17 summarizes the key considerations by LCOE driver.

⁷ At the time of data extraction, ERA5 had a spatial resolution of 0.5°. Data for the site at -124.71° W, 40.93° N were approximated using the a grid point at -125.00° W, 41.00° N.

Table 17. Summary of Design Basis Considerations by Key LCOE Driver

LCOE Driver	Assumptions
FCR	<ul style="list-style-type: none"> Pre-tax FCR was calculated without adjustments for depreciation, based on assumptions from [1], including an inflation rate of 2.5%, cost of debt of 5.9%, cost of equity of 9%, and a debt share of 60%.
CapEx	<ul style="list-style-type: none"> Supply CapEx (excluding installation) for mooring lines, anchors, and intra-array cables was derived from the design work in previous sections and design basis cost inputs. These values were included directly in the modeling rather than using the ORBIT model, which, as a medium-fidelity tool, may not fully reflect the specific design choices presented here. See the text below this table for further details on costs for the mooring lines, anchors, and intra-array system. Project development costs were set to 9.7% of CapEx, following [1] Interest during construction was set at 5.9%, consistent with the recommended cost of debt in [1].
OpEx	<ul style="list-style-type: none"> Fixed O&M costs were derived from [35], as recommended in [1]. Updated estimates of \$46/kW were used, covering insurance, lease fees, operating facilities, training, onshore logistics, technical resources, and administrative support, replacing the outdated \$31/kW estimate in [1].

The costs shown in Table 18, Table 19, and Table 20 correspond to the system designs developed and discussed in earlier sections of the report. The mooring line and cable material costs were from [1]. The cost of the clump weight in the mooring design was based on the reported \$0.576/kg cost of gravity anchors from [36]. The suction pile anchor costs shown in Table 19 reflect material and fabrication estimates only, based on indicative ranges reported in [1], and are included here solely for comparative purposes. Actual market prices are generally higher (approximately \$0.7–\$1 million), as they typically incorporate engineering, ancillary components, and additional indirect costs. The cost of the buoyancy modules was scaled to \$33,000 per 1-m³ module, based on the cost reported in [1] scaled using NLR’s 80-m-depth lazy-wave cable design in [22]. The dynamic cable cost per meter in Table 20 includes the cost of the buoyancy modules.

Table 18. Cost and Mass of Taut Line (Chain-Clump Weight-Polyester-Chain) With 1,400-m Anchoring Radius

Mooring Cost/Line (USD)	Total Wind Farm Mooring Cost (USD)	Mooring Mass/Line (kg)	Mooring Mass/Line (tonnes)
528,126	106,153,343	127,004	127

Table 19. Cost and Mass of Suction Pile Anchor

Anchor Cost (USD)	Total Wind Farm Anchor Cost (USD)	Anchor Mass (tonnes)
338,391	68,016,491	76.3

Table 20. Cost and Mass of 66-kV Array Cables

Cable Conductor Area (mm ²)	Dynamic Cable Cost (USD/m)	Static Cable Cost (USD/m)	Dynamic Cable Total Length (m)	Static Cable Total Length (m)	Connector Cost/cable (USD)	Joint Cost/cable (USD)	# of Cables	Total Wind Farm Cable Cost (USD)	Total Wind Farm Cable Mass (kg)
300 suspended	985	-	72,202	-	203,000	-	39	79,008,808	3,115,223
630 suspended	1,621	-	30,078	-	273,000	-	18	53,683,486	2,074,589
1,000 suspended	2,398	-	1,704	-	352,000	-	1	4,437,255	162,645
300 lazy	1,172	500	6,047	78	203,000	237,000	2	8,006,139	280,998
630 lazy	1,848	655	9,070	15,816	273,000	237,000	3	28,652,622	1,358,909
1,000 lazy	2,745	959	12,094	4,488	352,000	237,000	4	39,853,905	1,437,832
Total								213,642,682	8,430,197

7.3 Results

This subsection presents the results for FCR, CapEx, OpEx, net AEP, and LCOE.

7.3.1 FCR

As discussed in Section 7.2, FCR estimates are primarily driven by inputs from [1] and calculated without adjustments for depreciation or taxes. Table 21 summarizes the parameters and resulting FCR outputs.

Table 21. Inputs and Outputs Used To Derive FCR

Parameter	Value
Project design life	25 years
Tax rate (combined state and federal) ^a	0%
Inflation rate	2.5%
Debt fraction	60.0%
Debt interest rate (nominal)	5.9%
Return on equity (nominal)	9.0%
WACC (nominal; pre-tax)	7.14%
WACC (real; pre-tax)	4.53%
Capital recovery factor (nominal; pre-tax)	8.69%
Capital recovery factor (real; pre-tax)	6.76%
Depreciation adjustment (net present value) ^a	100%
Project finance factor	100%
FCR (nominal)	8.69%
FCR (real)	6.76%

^a The values for tax rate and depreciation adjustment reflect the assumption that the design basis excludes tax and depreciation.

7.3.2 CapEx

Table 22 presents the CapEx breakdown from ORBIT, with the final column describing how each cost was modeled. Figure 25 illustrates the same data as a donut chart for visual reference.

Table 22. CapEx Breakdown in 2024 USD

Component	Category	Value (\$/kW)	How was it modeled?
Turbine	Turbine	1,770	ORBIT input based on [27]
Substructure	BOS CapEx	1,244	ORBIT output
Substructure installation	BOS CapEx	264	ORBIT output
Mooring system	BOS CapEx	173	ORBIT input based on Section 7.2.2
Mooring system installation	BOS CapEx	57	ORBIT output, mass from Section 7.2.2
Array system	BOS CapEx	213	ORBIT input based on Section 7.2.2
Array system installation	BOS CapEx	160	ORBIT output
Offshore substation (OSS)	BOS CapEx	234	ORBIT output
OSS installation	BOS CapEx	5	ORBIT output
Export system	BOS CapEx	240	ORBIT output
Export system installation	BOS CapEx	181	ORBIT output
Onshore substation	BOS CapEx	145	ORBIT output
Project development	BOS CapEx	642	ORBIT output
Commissioning	Soft CapEx	58	ORBIT output
Construction financing	Soft CapEx	516	ORBIT output
Construction insurance	Soft CapEx	104	ORBIT output
Decommissioning	Soft CapEx	133	ORBIT output
Procurement contingency	Soft CapEx	251	ORBIT output
Installation contingency	Soft CapEx	230	ORBIT output
Grid/network upgrades	Other CapEx	-	Not modeled in ORBIT
Supply chain, port dev.	Other CapEx	-	Not modeled in ORBIT
Total	-	6,620	-

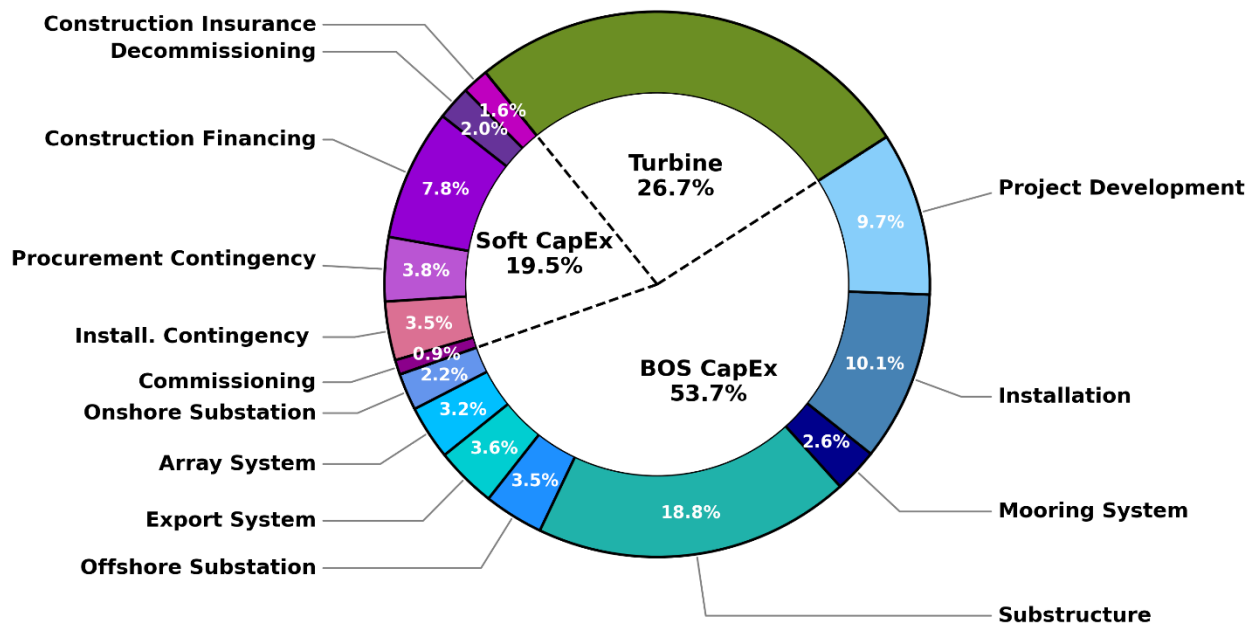


Figure 25. CapEx donut chart, showing each component’s share of total CapEx

The resulting CapEx of \$6,620/kW (2024 USD) excludes potential grid/network upgrades as well as supply chain and port development costs. These costs may represent additional burdens in regions where network upgrades beyond the POI may not be financed by the transmission system operator, or in less mature markets where suppliers and port authorities may lack the long-term demand certainty to invest in infrastructure and manufacturing without developer support. These exclusions allow CapEx to remain directly comparable across designs in different regions, but they should be included when estimating the CapEx of an actual project.

7.3.3 OpEx

Table 23 summarizes the OpEx breakdown derived from WOMBAT, with the final column describing how each cost was modeled.

Table 23. OpEx Breakdown in 2024 USD

Component	Category	Value (\$/kW-year)	How was it modeled?
Labor (technicians)	Maintenance	5.1	WOMBAT input based on assumed # of year-round full-time technicians (30)
Materials	Maintenance	3.1	WOMBAT output
Equipment (vessels)	Maintenance	29.8	WOMBAT output
AHT	Maintenance	3.3	WOMBAT output
CLV	Maintenance	16.0	WOMBAT output
CTV 1	Maintenance	1.2	WOMBAT output
CTV 2	Maintenance	1.2	WOMBAT output
CTV 3	Maintenance	1.2	WOMBAT output
DSV	Maintenance	1.7	WOMBAT output
Tugboat Group 1	Maintenance	2.7	WOMBAT output
Tugboat Group 2	Maintenance	2.7	WOMBAT output
Port fees	Operations	10.7	WOMBAT input based on repair time at port and monthly port fee from [28]
Insurance	Operations	17.9	WOMBAT input from [35]
Lease fees	Operations	3.0	WOMBAT input based on [37],[38]
Operating facilities	Operations	1.7	WOMBAT input from [35]
Other	Operations	23.5	WOMBAT input from [35]
Total	-	94.9	-

AHT = anchor handling tug; CLV = cable lay vessel; CTV = crew transfer vessel; DSV = diving support vessel; Other includes training, onshore logistics, technical resource, and administrative and support staff.

7.3.4 Net AEP

Table 24 presents the loss breakdown from WAVES, showing how the net capacity factor was derived from the gross capacity factor calculated in FLORIS.

Table 24. Breakdown of Losses From Gross to Net Generation

Parameter	Units	Value	How was it modeled?
Gross capacity factor	%	61.3%	FLORIS output
Total losses	%	17.6%	WAVES output
Availability losses	%	7.1%	WOMBAT output, production-based
Electrical losses	%	3.8%	WAVES output based on cable distance
Environmental losses	%	1.6%	WAVES default input
Technical losses	%	1.2%	WAVES default input
Wake losses (internal)	%	5.1%	FLORIS output
Net capacity factor	%	50.6%	WAVES output
Net AEP per kW	MWh/kW	4.432	WAVES output

7.3.5 LCOE

Figure 26 presents the LCOE breakdown for all CapEx and OpEx components, incorporating financing assumptions and net AEP. The resulting LCOE of \$122.4/MWh (real 2024 USD) excludes potential grid/network upgrades, as well as supply chain and port development costs that may be required in less mature markets. These exclusions ensure that the LCOE remains directly comparable to other designs in different regions, but they should not be omitted when calculating the LCOE of an actual project.

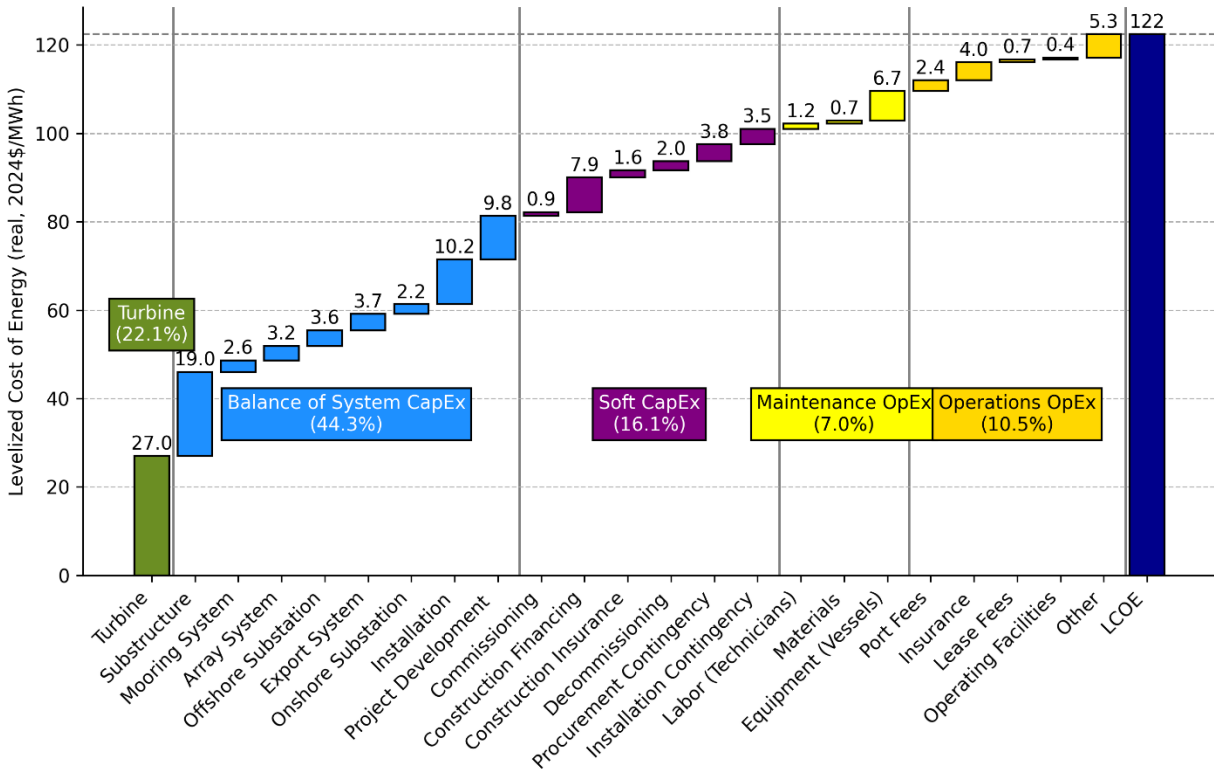


Figure 26. LCOE waterfall in real 2024 USD

8 Conclusion

IEA Wind Task 49 collaboratively developed a deep-water floating wind array design, the IEA Wind RFA3, with the goal of providing a reference to inform future floating wind research efforts. The deep-water array consists of the design of the floating components: mooring system, anchors, cables and the array layout and cable routing. The designs were iteratively developed through coordinated research efforts across several countries, following best practices and design requirements that were previously outlined within the Task 49 design basis.

Following the initial Task 49 scoping, the design is a 1-GW farm composed of IEA Wind 15-MW reference wind turbines and VoltturnUS-S semisubmersible platforms. The array is designed for Humboldt site conditions and a uniform 800-m depth.

The deep-water design features taut mooring systems composed of chain and polyester, with a clump weight along the polyester. Dynamic performance results show that the mooring design meets requirements around maximum allowable tension and fatigue damage, while avoiding slack loads. The anchor design is a steel suction caisson, with the dimensions optimized to satisfy loading requirements. The dynamic cable designs are sized for three conductor sizes (300, 630, and 1,000 mm²) and include both fully suspended and lazy-wave profiles. The cable designs satisfy constraints on maximum tension and curvature in dynamic simulations. The array layout is a rectangular grid within a square lease area, sized to match the Humboldt northeast lease area. The turbine spacing was selected to maximize spacing in the predominant wind direction of due north. The cable routing selects the appropriate cable size based on the number of turbines in series, and routes along turbine rows toward a substation located on the east side of the array.

The cost and logistics modeling evaluates the economic performance of the Task 49 deep-water array, accounting for the specific mooring, cable, and layout design characteristics in its cost and wake-loss modeling. Using process-based installation and O&M logistics models alongside wake and AEP simulations, the analysis provides estimates of financial metrics, capital and operational expenditures, and energy generation. The modeled LCOE for the 1-GW floating wind farm is \$122.4/MWh (real 2024 USD), providing a representative benchmark for assessing alternative array designs.

To facilitate use of the design, we provide various design input files in a dedicated GitHub repository under the IEA Wind Task 49 GitHub organization [39]. This includes a yaml description of the full array in the Task 49 Ontology format, OpenFAST input files of the mooring system and dynamic cable designs, and cost model input files.

This reference design can serve as a baseline or starting point for future research efforts investigating floating wind arrays in deep water. With the provided mooring, cable, and array design details, users can directly adopt these designs in future studies. The cost modeling results provide a benchmarking data point that alternative array designs can compare against.

References

- [1] Hall, M., E. Lozon, F. Devoy McAuliffe, M. Baudino Bessone, I. Bayati, M. Bowie, P. Bozonnet, et al. 2024. *The IEA Wind Task 49 Reference Floating Wind Array Design Basis*. Golden, CO: National Renewable Energy Laboratory. NREL/TP-5000-89709. <https://docs.nlr.gov/docs/fy24osti/89709.pdf>.
- [2] Gaertner, E., J. Rinker, L. Sethuraman, F. Zahle, B. Anderson, G. Barter, N. Abbas, et al. 2020. *Definition of the IEA 15-Megawatt Offshore Reference Wind Turbine*. Golden, CO: National Renewable Energy Laboratory. NREL/TP-5000-75698. <https://docs.nrel.gov/docs/fy20osti/75698.pdf>.
- [3] Allen, C., A. Viselli, H. Dagher, A. Goupee, E. Gaertner, N. Abbas, M. Hall, and G. Barter. 2020. *Definition of the UMaine VoltturnUS-S Reference Platform Developed for the IEA Wind 15-Megawatt Offshore Reference Wind Turbine*. Golden, CO: National Renewable Energy Laboratory. NREL/TP-5000-76773. <https://docs.nrel.gov/docs/fy20osti/76773.pdf>.
- [4] Biglu, M., M. Hall, E. Lozon, and S. Housner. 2024. *Reference Site Conditions for Floating Wind Arrays in the United States*. Golden, CO: National Renewable Energy Laboratory. NREL/TP-5000-89897. <https://docs.nrel.gov/docs/fy24osti/89897.pdf>.
- [5] Biglu, M., M. Hall, E. Lozon, and S. Housner. 2024. “Reference Site Condition Datasets for Floating Wind Arrays in the United States.” NLR Data Catalog. Golden, CO: National Laboratory of the Rockies. Last updated: February 24, 2026. DOI: 10.7799/2425969.
- [6] Creane, S., P. Santos, K. Kölle, D. Airoidi, M. Bakhoday-Paskyabi, M. Biglu, W. Brown, et al. 2024. *Reference Site Conditions for Floating Wind Arrays*. Golden, CO: National Renewable Energy Laboratory. NREL/TP-5000-89937. <https://docs.nlr.gov/docs/fy24osti/89937.pdf>.
- [7] C. B. Devantier, X. H. Wong, and V. Schrameyer. 2024. “Marine growth along the mesopelagic zone.” DHI Technical Report. <https://doi.org/10.5281/zenodo.12731585>.
- [8] American Bureau of Shipping (ABS). 2020. *Guide for Building and Classing Floating Offshore Wind Turbines*. Spring, TX: American Bureau of Shipping. <https://ww2.eagle.org/content/dam/eagle/rules-and-guides/current/offshore/fowt-guide-july20.pdf>.
- [9] Hsu, W.-T., K.P. Thiagarajan, M. Hall, M. MacNicoll, and R. Akers. 2014. “Snap Loads on Mooring Lines of a Floating Offshore Wind Turbine Structure.” Proceedings of the ASME 2014 33rd International Conference on Offshore Mechanics and Arctic Engineering, June 8–13, 2014, San Francisco, CA. <https://doi.org/10.1115/OMAE2014-23587>.
- [10] Hall, M., S. Housner, S. Srinivas, and S. Wilson. 2021. *MoorPy: Quasi-Static Mooring Analysis in Python*. National Renewable Energy Laboratory. <https://doi.org/10.11578/dc.20210726.1>.

- [11] Hall, M., B. Duong, and E. Lozon. 2024. “Streamlined Loads Analysis of Floating Wind Turbines With Fiber Rope Mooring Lines.” Proceedings of the ASME 2023 5th International Offshore Wind Technical Conference. Dec. 18–19, 2023, Exeter, UK. <https://doi.org/10.1115/IOWTC2023-119524>.
- [12] DNV. 2021. DNV-OS-E301: “Position Mooring.” Available from dnv.com.
- [13] Jensen, N.O. 1983. *A Note on Wind Generator Interaction*. Roskilde, Denmark: Risø National Laboratory. https://backend.orbit.dtu.dk/ws/files/55857682/ris_m_2411.pdf.
- [14] Katic, I., J. Højstrup, and N.O. Jensen. 1987. “A Simple Model for Cluster Efficiency.” In W. Palz and E. Sesto (Eds.), *EWEC’86 Proceedings Vol. 1*, 407–410. https://backend.orbit.dtu.dk/ws/files/106427419/A_Simple_Model_for_Cluster_Efficiency_EWEC_86.pdf.
- [15] Aubeny, C. 2020. *Geomechanics of Marine Anchors*. CRC Press.
- [16] Lee, J., and C.P. Aubeny. 2025. “Optimal Design of a Deeply Embedded Ring Anchor System in Sand.” *Geotechnical Frontiers 2025*. <https://doi.org/10.1061/9780784485972.016>.
- [17] Tajalli Bakhsh, T., M. Monim, K. Simpson, T. Lapierre, J. Dahl, J. Rowe, and M. Spaulding. 2020. *Potential Earthquake, Landslide, Tsunami and Geo-Hazards for the U.S. Offshore Pacific Wind Farms*. Camarillo, CA: Bureau of Ocean Energy Management. BOEM/BSEE E17PS00128. <https://www.rpsgroup.com/imported-media/5565/potential-earthquake-landslide-tsunami-and-geohazards-for-the-us-offshore-pacific-wind-farms.pdf>.
- [18] American Petroleum Institute (API). 2005. APO RP 2SK: “Design and Analysis of Stationkeeping Systems for Floating Structures.
- [19] Aubeny, C.P., S.W. Han, and D. Murff. 2003. “Inclined Load Capacity of Suction Caissons.” *International Journal for Numerical and Analytical Methods in Geomechanics* 27(14): 1235–1254. <https://doi.org/10.1002/nag.319>.
- [20] Hall, M., and A. Goupee. 2015. “Validation of a Lumped-Mass Mooring Line Model With DeepCwind Semisubmersible Model Test Data.” *Ocean Engineering* 104: 590–603. <https://doi.org/10.1016/j.oceaneng.2015.05.035>.
- [21] Hall, M., S. Srinivas, and Y.-H. Yu. 2020. *Implementation and Verification of Cable Bending Stiffness in MoorDyn: Preprint*. Golden, CO: National Renewable Energy Laboratory. NREL/CP-5000-76968. <https://www.nrel.gov/docs/fy21osti/76968.pdf>.
- [22] Lozon, E., M. Reddy Lekkala, L. Sirkis, and M. Hall. 2025. “Reference Mooring and Dynamic Cable Designs for Representative U.S. Floating Wind Farms.” *Ocean Engineering* 322: 120473. <https://doi.org/10.1016/j.oceaneng.2025.120473>.
- [23] Jonkman, B., A. Platt, R.M. Mudafort, E. Branlard, M. Sprague, H. Ross, J. Jonkman, et al. “OpenFAST/openfast: v3.5.2.” <https://ui.adsabs.harvard.edu/abs/2024zndo..10530537J/abstract>.

- [24] Hall, M., M. Biglu, S. Housner, K. Coughlan, M. Y. Mahfouz, and E. Lozon. 2024. “Floating Wind Farm Layout Optimization Considering Moorings and Seabed Variations.” *Journal of Physics: Conference Series* 2767: 062038. <https://doi.org/10.1088/1742-6596/2767/6/062038>.
- [25] Nassor, A., Y. Alkarem, M. Castagne, M. Hall, J. Lee, E. Lozon, P. Malisani, Y. Poirrette, and V. Ramachandran. 2025. “Floating Offshore Wind Farm Design Optimization, Including Mooring Line Orientations and Fatigue Design.” ASME 2025 International Offshore Wind Technical Conference, Oct. 27–29, 2025, Toulon, France. <https://doi.org/10.1115/IOWTC2025-165418>.
- [26] National Laboratory of the Rockies. 2024. “Annual Technology Baseline – Financial Cases and Methods.” https://atb.nrel.gov/electricity/2024/financial_cases_&_methods.
- [27] Stehly, T., P. Duffy, and D. Mulas Hernando. 2024. “Cost of Wind Energy Review: 2024 Edition.” National Renewable Energy Laboratory. NREL/PR-5000-91775. <https://www.osti.gov/servlets/purl/2479271/>.
- [28] National Laboratory of the Rockies. No date. “Offshore Renewable Balance-of-system Installation Tool (ORBIT).” <https://github.com/NLRWindSystems/ORBIT>.
- [29] National Laboratory of the Rockies. No date. “Windfarm Operations & Maintenance cost-Benefit Analysis Tool.” <https://github.com/NLRWindSystems/WOMBAT>.
- [30] National Laboratory of the Rockies. No date. “FLORIS.” <https://github.com/NatLabRockies/floris>.
- [31] National Laboratory of the Rockies. No date. “Offshore Wind Farm Lifecycle Estimation.” <https://github.com/NatLabRockies/WAVES>.
- [32] California Energy Commission. 2024. *Substation Planning Evaluation-Humboldt Wind Energy Area*.” TN#258389. Available at <https://efiling.energy.ca.gov/Lists/DocketLog.aspx?docketnumber=17-MISC-01>.
- [33] Crowley. 2022. “Crowley, Humboldt Bay to Develop and Operate California Wind Terminal.” <https://www.crowley.com/news-and-media/press-releases/humboldt-bay-wind/>.
- [34] ECMWF. 2023. “ERA5 Hourly Data on Single Levels From 1940 to Present.” <https://doi.org/10.24381/cds.adbb2d47>.
- [35] BVG Associates. No Date. “Wind Farm Costs.” In *Guide to a Floating Offshore Wind Farm*. <https://guidetofloatingoffshorewind.com/wind-farm-costs/>.
- [36] Davies, R., E. Baca, and M. Hall. 2025. “An Updated Mooring Cost Modeling Tool Set With Application to a Reference Model Wave Energy Converter.” Proceedings of ASME 2025 44th International Conference on Ocean, Offshore and Arctic Engineering, June 22–27, 2025, Vancouver, Canada. <https://doi.org/10.1115/OMAE2025-156384>.

[37] Bureau of Ocean Energy Management. 2014. “Commercial Lease of Submerged Lands for Renewable Energy Development on the Outer Continental Shelf.”
<https://www.boem.gov/sites/default/files/documents/oil-gas-energy/Lease-Issued.pdf>.

[38] National Laboratory of the Rockies. No date. “Scenario Viewer: Data Downloader – Cambium 2024.” <https://scenarioviewer.nrel.gov/>.

[39] Lozon, E., Ramachandran Nair Rajasree, V., Mulas Hernando, D., Lee, J., Castagné, M., Nassor, A., Poirette, Y., Alkarem, Y.R., Biglu, M., Sirkis, L.H., Hall, M., 2026. “The IEA Wind RFA3 Deep-Water Reference Array Design”. IEA Wind Task 49.
<https://doi.org/10.5281/zenodo.20218023>

Appendix A. Gumbel Distribution Fit for Extreme Tension Values

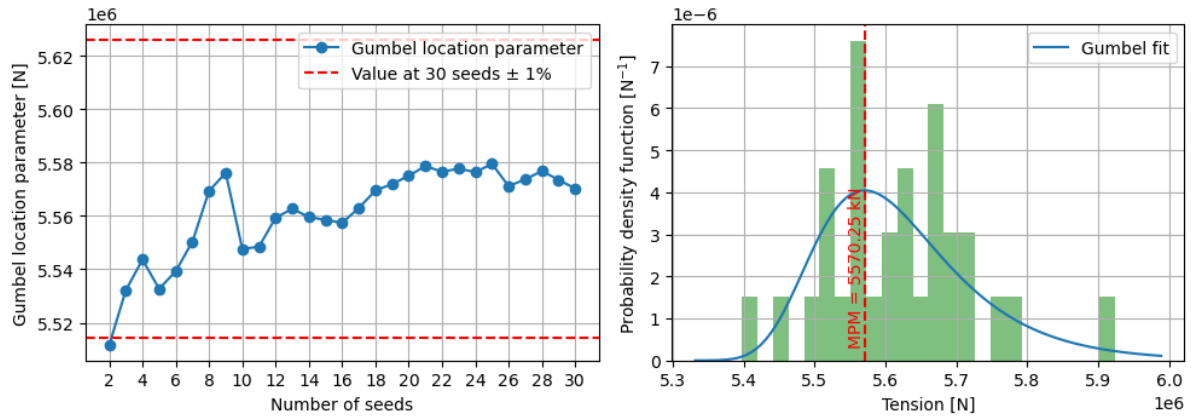


Figure A-1. Gumbel distribution fit for maximum tension in mooring line 2, DLC 1.6, 0°

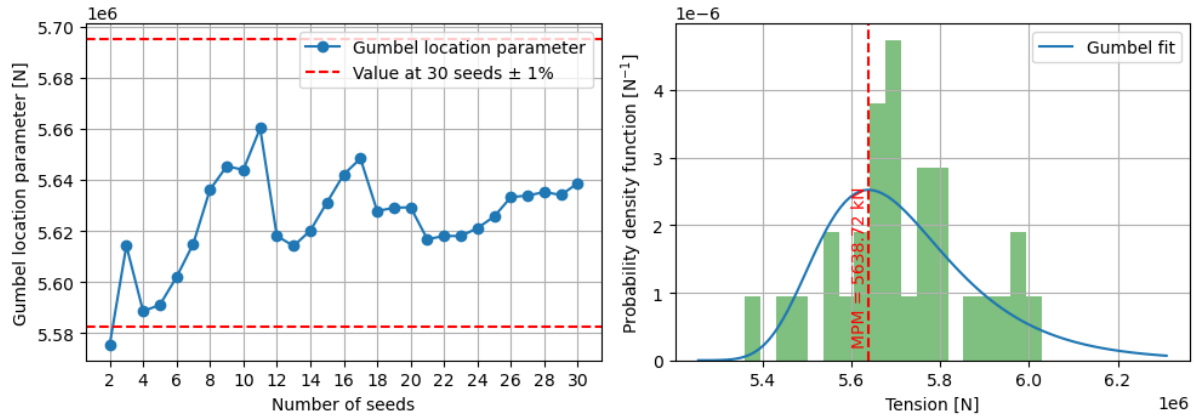


Figure A-2. Gumbel distribution fit for maximum tension in mooring line 2, DLC 6.1, 0°

Gumbel convergence plot for SLC 0°

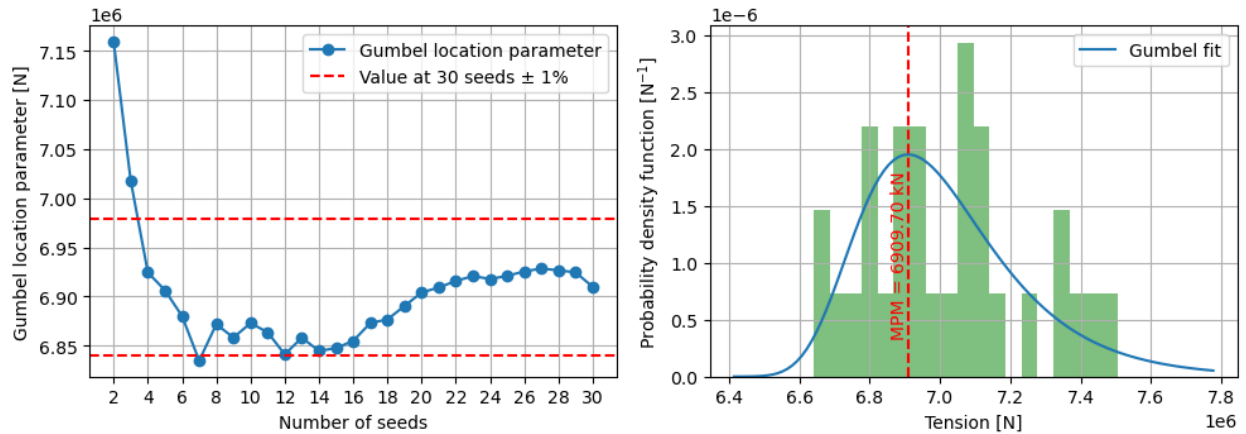


Figure A-3. Gumbel distribution fit for maximum tension in mooring line 2, SLC, 0°